(n, n', γ) REACTIONS WITH STABLE LIGHT NUCLEI, Z= 13 TO 17

(n, n', γ) REACTIONS WITH STABLE LIGHT NUCLEI IN THE REGION Z = 13 TO 17

by

PETER IRVIN CLAYTON ERNST, B.Eng.

A Thesis

Submitted to the Faculty of Graduate Studies

in Partial Fulfilment of the Requirements

for the Degree

Master of Science.

McMaster University

September, 1968.

MASTER OF SCIENCE (1968) McMASTER UNIVERSITY

(Physics) Hamilton, Ontario.

TITLE: (n, n', γ) Reactions with Stable Light Nuclei in the Region Z = 13 to 17.

AUTHOR: Peter Irvin Clayton Ernst, B.Eng. (McMaster University

SUPERVISOR: Dr. G. L. Keech

NUMBER OF PAGES: vii, 89

SCOPE AND CONTENTS:

This thesis describes the investigation of the γ-rays arising from the inelastic scattering of a fission produced neutron spectrum by stable light nuclei in the region Z = 13 to 17. The high resolution of a Ge(Li) detector was employed to indicate some discrepancies with previously reported data for the decay schemes of the above mentioned nuclei. The correlation between the primary population values of the levels and their spin and parity assignments was also considered.

ACKNOWLEDGEMENTS

I wish to express appreciation to my Research Director, Dr. G. L. Keech, for his patience and understanding throughout the preparations for this work.

In particular, I would also like to thank Dr. T. J. Kennett for his assistance and guidance, without which this work would not have been accomplished. My thanks also to Mr. H. Lycklama for the collection and partial reduction of the ^{31}P data presented herein and to Mr. G. R. Norman and Mr. L. N. Nichol for their kind assistance as well as to various other members of their group. Appreciation also goes to Mrs. E. Hall for speedy completion of a sometimes difficult typing job.

TABLE OF CONTENTS

LIST OF TABLES

LIST OF ILLUSTRATIONS

I INTRODUCTION

1.1 General

Inelastic scattering of nuclear particles from stable nuclides casts considerable light upon the properties of the target nucleus. For moderate particle energies in which only a few levels are excited, the total crossection as well as the energy and angular distribution of the emergent particles are sensitive to the energy, angular momentum, and parity differences which exist between the ground state of the target nucleus and the states excited. Measuring the energies of γ-rays arising from inelastic neutron scattering is particularly useful because of the precision of the γ-ray energy measurements one is now able to obtain with solid state detectors. This present work was performed to check on the practicality of using a reactor produced neutron spectrum to excite stable light nuclei in order to compare their excitation level structures with previous work performed by other methods. The correlation between the crossection for exciting a particular state by neutron inelastic scattering and its spin and parity was also considered. The seemingly observed correlations were then used to predict spin values for excited states for which J^{π} values have not as yet been assigned. Light nuclei were chosen because of their relatively uncomplicated and well known level structures.

The use of inelastic neutron scattering vs inelastic charged particle scattering gives unambiguous results since no corrections need be made for coulomb factors, but has the disadvantage that

neutron energies cannot be measured with as good resolution as charged particles. By observing the γ-rays from inelastic neutron scattering one uses the advantage of (n, n') scattering and overcomes its resolution shortcomings by employing good resolution solid state γ-ray detectors now available.

1.2 Neutron Sources

The selection of the most desireable source of neutrons is dependent upon the nature of the information desired. Through the use of charged particle reactions it is possible to produce intense sources of fixed neutron energy or variable energy at much diminished intensity.

A second source of neutrons which is very intense but which leads to a continuous energy distribution is that obtained from the fission reaction. For energies above about 2 Mev (12) this spectrum can be approximated by

$$\Phi(E) = \Phi_0 e^{-\alpha E} \qquad (1.1)$$

One of the advantages of a reactor produced neutron spectrum is that all levels can be populated concurrently although, admittedly, with much less probability at higher energies. With accelerator produced neutrons one can only observe levels below the neutron energies available.

The form of the neutron inelastic scattering crossection plays an important role in the choice of the desired neutron spectrum. In general, this crossection rises rapidly with neutron energy from zero at the level threshold to nearly a constant. This is approximated

by Donahue (2) as

$$\sigma(E) = \sigma_\infty (1 - e^{-\beta (E - E_{th})}) \qquad (1.2)$$

where σ_∞ is a constant dependent on the J^π value of the excited level. A value of β which is consistant with most available measurements is $\beta = 3 \pm 1$ Mev^{-1} as given in Reference (2).

One now looks at how the reaction rate, R(E), varies with energy and sees that using a reactor produced neutron spectrum it is going to be of the form

$$R(E) \sim \sigma(E)\, \Phi(E) \qquad (1.3)$$

Using equations (1.1) and (1.2) this expands to

$$R(E) \sim \sigma_\infty \Phi_0 (1 - e^{-\beta (E - E_{th})}) e^{-\alpha E} \qquad (1.4)$$

A plot of this curve for a threshold energy of 2 Mev, i.e. $E_{th} = 2$, is given in Figure 1-1. From the curve one can see that the mean reaction rate for this combination of flux distribution and crossection variation occurs about 0.5 Mev above the threshold, a region in which the crossection for the reaction is most dependent on the spin and parity of the level concerned. One also sees that from about 1.5 Mev above the threshold the curve follows the flux distribution curve.

The above considerations coupled with the good intensity of neutrons available from a reactor, make the reactor produced source advantageous. The disadvantages of uncertainties in flux distribution are somewhat overcome by the capability of performing long uninterrupted runs to provide good statistics.

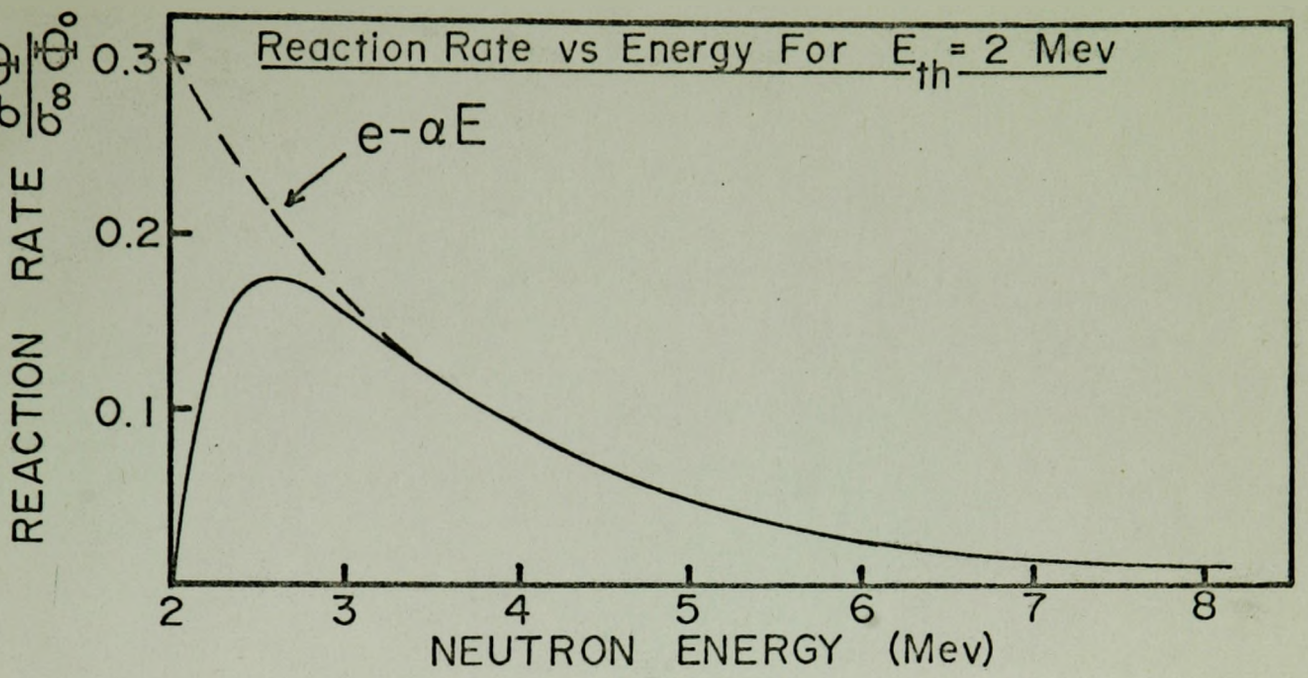

FIGURE 1-1

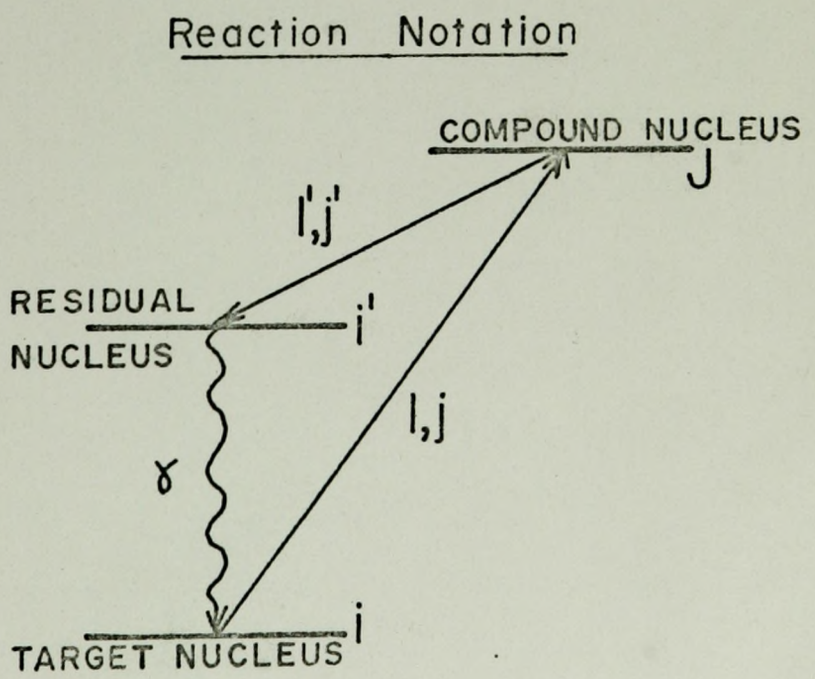

FIGURE 1-2

1.3 Reaction Mechanism

(a) Notation (1)

Referring to Figure 1-2, let the target nucleus have a spin of i (in units of h), the residual nucleus a spin of i', the initial and final orbital neutron angular momentum by ℓ and ℓ', respectively, the corresponding initial and final energies E and E'. The spin of a level in the compound nucleus will be donated by J. It is convenient to combine the neutron spin and the spin of the nucleus to form the channel spins j and j' for the initial and final states.

$$j = i \pm 1/2, \quad j' = i' \pm 1/2 \qquad (1.5)$$

The spin of the compound nucleus J is formed by combining ℓ and j or ℓ' and j'. For a given value of J the values of ℓ and ℓ' which may contribute to a reaction are given by

$$|J - j| \leq \ell \leq (J + j), \quad |J - j'| \leq \ell' \leq (J + j') \qquad (1.6)$$

Parity must, of course, be conserved. Changes in parity will be carried by the neutron orbital angular momenta, even ℓ and ℓ' corresponding to no change in parity with odd ℓ and ℓ' introducing a parity change.

The γ-ray shown in Figure 1-2 represents the de-excitation of the excited state of the target nucleus. This may be either a single γ-ray or a cascade and represents the total photon energy seen in a (n, n', γ) reaction. This radiation, $\Delta\ell$-pole, is such that $\Delta\ell \leq |i - i'|$.

(b) Simplifications from the Statistical Model

Previously one has assumed a simple representation of the inelastic

neutron scattering crossection as given in equation (1.2). A more rigorus formula is given by Hauser and Feshbach (1), employing the statistical model with some simplifications.

Assuming all interference terms vanish as discussed in (1) one may write

$$\sigma(i \mid i') = \frac{\pi\lambda^2}{2(2\ i + 1)} \sum_{l, l', j'} T_l(E)\, T_{l'}(E)(2J+1)\epsilon^{J}_{j,l}\epsilon^{J}_{j,l'} \quad (1.7)$$

where the $\epsilon_{j,l}\ J = \begin{cases} 2 \text{ if both } j_1 \text{ and } j_2 \\ 1 \text{ if } j_1 \text{ or } j_2, \text{ but not both} \\ 0 \text{ if neither } j_1 \text{ nor } j_2 \end{cases}$

satisfy the condition

$$\left| J - l \right| \leq j_i \leq (J + l). \qquad (1.8)$$

In the above equation $T_l(E)$ and $T_{l'}(E)$ are the transmission coefficients, for the particular compound nucleus involved, of the entering and leaving neutrons. Equation (1.7) follows from equation (9) of Feshbach (1) by eliminating the primed sum in the denominator of equation (9) to simplify calculations.

The above formula applies to even-even nuclei only and must be so recognized.

In order to calculate an example one must construct a table similar to Table I-1 to get the values necessary. This table was set up to demonstrate the calculation of $\sigma(0^+ \mid 2^+)$ for the $0^+ \rightarrow 2^+$ reaction. The table demonstrates the many ways one might form the compound nucleus and the neutron wave numbers so involved.

1.4 Primary Population Values for Excited States

(a) According to Hauser and Feshbach (1)

One can calculate the expected relative primary population value

TABLE I-1

NEUTRON ANGULAR MOMENTA INVOLVED IN A $0^+ \rightarrow 2^+$ EXCITATION.

J	l	$\epsilon_{j,l}^{J}$	l'	$\epsilon_{j',l'}^{J}$	Neutron Waves n-n'
$1/2^+$	0	1	2	2	s-d
$1/2^-$	1	1	1	1	p-p
			3	2	p-f
$3/2^-$	1	1	1	2	p-p
			3	2	p-f
$3/2^+$	2	1	0	1	d-s
			2	2	d-d
			4	1	d-g
$5/2^+$	2	1	0	1	d-s
			2	2	d-d
			4	2	d-g
$5/2^-$	3	1	1	2	f-p
			3	2	f-f
			5	1	f-h

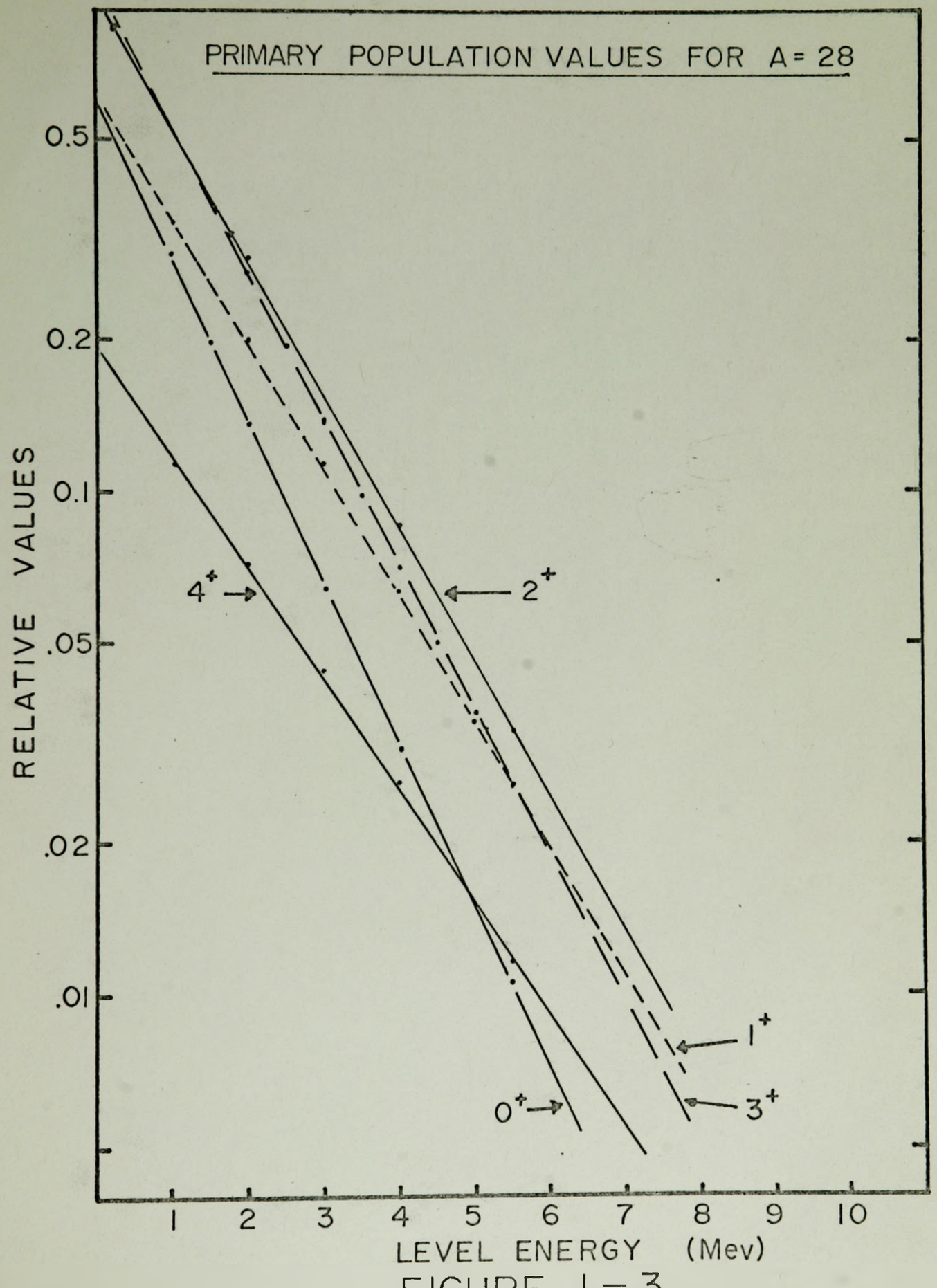
PRIMARY POPULATION VALUES FOR A = 28
RELATIVE VALUES
0.5
0.2
0.1
.05
.02
.01
4+
2+
1+
3+
0+
1
2
3
4
5
6
7
8
9
10
LEVEL ENERGY (Mev)

FIGURE 1-3

for a particular level of a even-even nucleus from

$$P_{i'} = \int_{E_{th}}^{\infty} \sigma(i \mid i') \, \bar{E}_o \, e^{-\alpha E} \, dE \qquad (1.9)$$

where $P_{i'}$ is the relative primary population value for excited state i' of the nucleus. If one carries out the calculations for many values of E' one obtains a curve of the relative primary population values for a level of given spin and parity vs level energy. By using different values of i' one can obtain a family of curves for different J^{π} values. Since the transmission coefficients of equation (1.7) vary with mass number one may not use this family of curves for other than the nucleus mass considered in the calculations of the transmission coefficients. For these reasons it is desireable to use the advantages of a computer programme to carry out the calculations. These have been done (13) for mass 28 as shown in Figure 1-3 where it is seen that the $0^+ \longrightarrow 2^+$ excitations are the most probable for a given energy. For clarity only the positive parity states are shown. The negative states, in general, follow the same slope as their corresponding positive states and lie just below them except for 1^- and 4^- which are above.

(b) <u>According to Donahue (2)</u>

Donahue's simplifications of the crossection representation allow one to make simple calculations without involving a computer. The relative primary population values or total reaction rate is obtained from equation (1.4) by

$$P_i(E_{th}) = \int_{E_{th}}^{\infty} R(E)\, dE$$

$$= \int_{E_{th}}^{\infty} \sigma_{\infty i}\, \Phi_0 \left(1 - e^{-\beta(E-E_{th})}\right) e^{-\alpha E} dE$$

$$= \sigma_{\infty i}\, \Phi_0 \frac{\beta}{\alpha(\alpha+\beta)}\, e^{-\alpha E_{th}} \qquad (1.10)$$

where it is stressed that $\sigma_{\infty i}$ is the limiting value assumed for the crossection of a level with spin and parity i. Since one is dealing in relative values one may write

$$P_i(E_{th}) \sim e^{-\alpha E_{th}} \qquad (1.11)$$

which is a simple exponential. If one corrects the relative population values observed for flux and crossection variations using

$$P_i(\text{corrected}) = \frac{P_{ob}}{P_i(E_{ob})}, \qquad (1.12)$$

where P_i (corrected) is the corrected relative primary population value, P_{ob} is the observed value and $P_i(E_{ob})$ is the relative primary population value calculated from (1.11), one should obtain a plot of corrected values vs level energies. Theoretically, one should be able to draw a horizontal line through corrected values of levels with the same J^{π} values. One then has a series of horizontal lines, one for each J^{π} value.

It now remains to use the above ideas in an experiment to see which seems more valid.

CHAPTER II

EXPERIMENTAL PROCEDURES

2.1 Targets

This investigation was carried out on the stable nuclides for elements with Z=13 to 17, aluminum to chlorine. The physical characteristics of the targets used are tabulated in Table II-1. Naturally high purity targets are required since impurities can result in a misinterpretation of the measurements. Figure 2-1 shows one the relative isotopic abundances and nuclear stabilities involved for these elements.

TABLE II-1

TARGET CHARACTERISTICS

Element to be studied	Target Form	Container (if any)	Size	Weight	Volume
Al	metal	--------	2 cm Dia. x 8 cm long	70 gm	25 cc
Si	metal	--------	2 cm Dia. x 10 cm long	81 gm	30 cc
P	red phosphorus powder	paper tube	2 cm Dia. x 8 cm	30 gm	25 cc
S	powder	paper tube	2 cm Dia. x 10 cm	27 gm	30 cc
Cl	CCl_4 liquid	2 poly vials	2 (2.2 cm Dia. x 3.8 cm long)	42 gm	28 cc

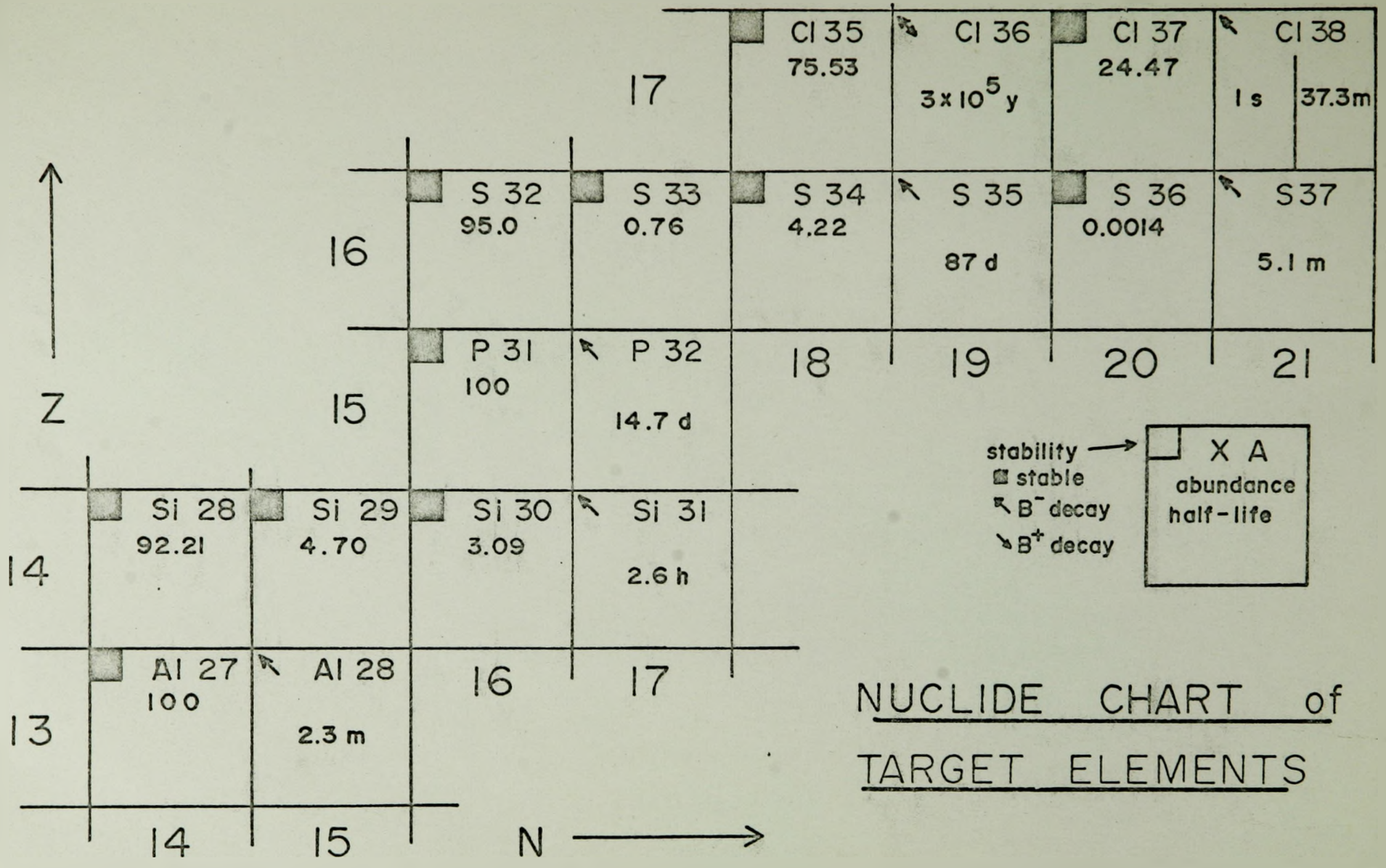
Cl 35
75.53
Cl 36
3x10^5 y
Cl 37
24.47
Cl 38
1 s
37.3m
17
S 32
95.0
S 33
0.76
S 34
4.22
S 35
87 d
S 36
0.0014
S37
5.1 m
16
P 31
100
P 32
14.7 d
15
18
19
20
21
Z
Si 28
92.21
Si 29
4.70
Si 30
3.09
Si 31
2.6 h
14
Al 27
100
Al 28
2.3 m
13
16
17
14
15
N
stability
stable
B⁻ decay
B⁺ decay
X A
abundance
half-life
NUCLIDE CHART of
TARGET ELEMENTS

FIGURE 2-1

2.2 Apparatus

Reactor produced neutrons as available at Beam Port Number 1 of the McMaster Nuclear Reactor were used for the present work. This beam port facility, as previously described by Johns *et al*[3], is shown in Figure 2-2. The dewar was not used as such and all but one of the quartz crystal filters were removed for this experiment in order to enhance the fast neutron component. To reduce the thermal neutron flux in the beam a boron loaded polyethylene shutter behind the dewar was left closed, except during the thermal calibration runs.

To aid in containing neutrons scattered from the beam a boron lined collimator was placed just outside the beam port shielding and aligned with the beam. This collimator consisted of a concentric arrangement of a 1" I.D. x 1/8" thick wall plastic tube inside another 1 3/4" O.D. x 1/8" thick wall plastic tube with the resulting 1/4 inch annulus inbetween filled with boron carbide and sealed at the ends.

The targets, mentioned previously, were located inside this collimator and observed by a coaxial Lithium-drifted Germanium, Ge(Li), solid state γ-ray detector. The detector used in this instance was approximately 15 cc in volume and operated at liquid nitrogen temperature with approximately 750 volts of reverse bias. Further explanation of this type of detector and its arrangement can be found in reference (4). The position of the detector was such that the angle between the beam axis, centre of sample, and detector was 90°.

The output pulses from the detector were amplified by a Tennelec TC130C FET preamplifier and a TC200 linear amplifier. Pulse-height analysis for each run was performed using 4096 channels of a

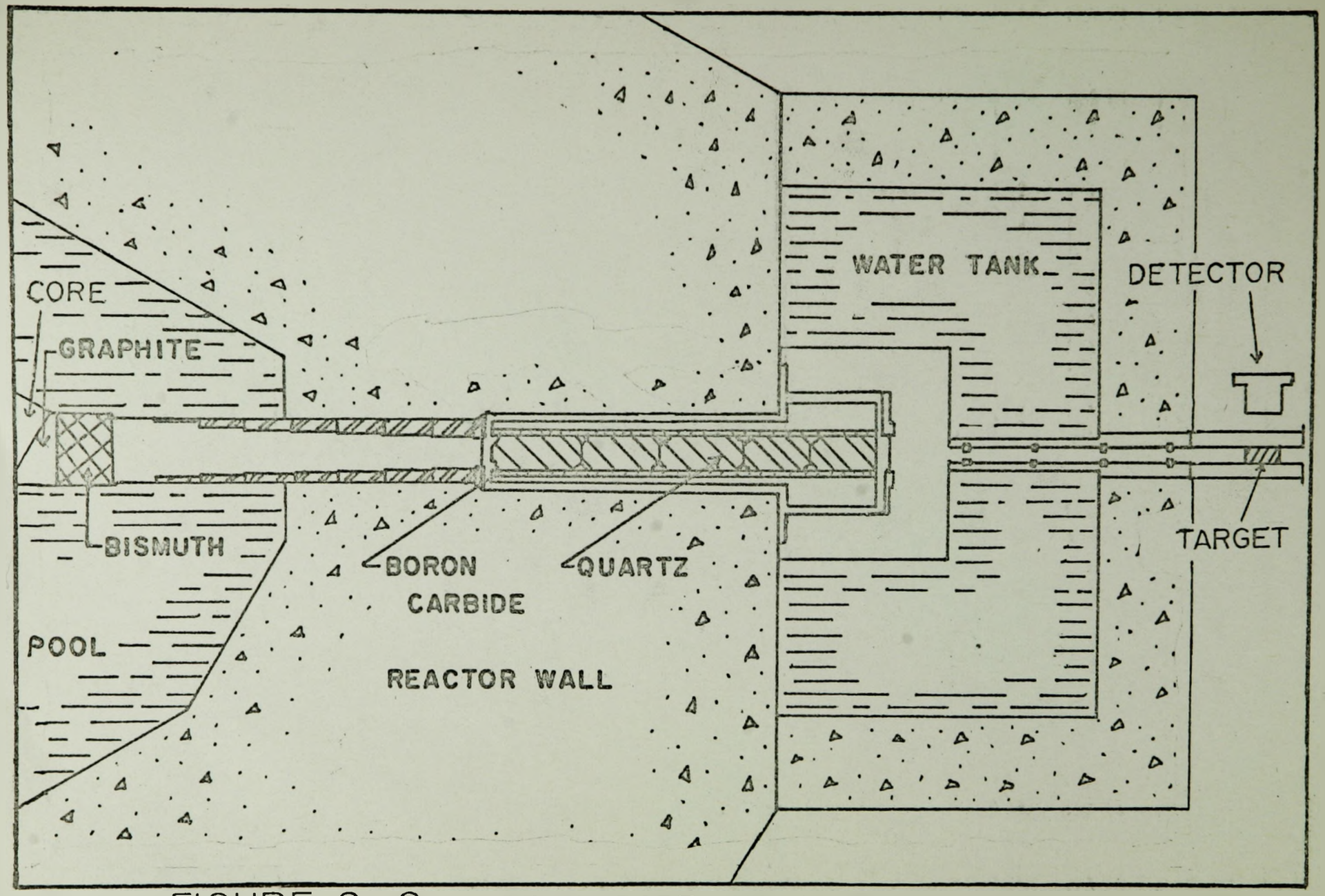

FIGURE 2-2. BEAM PORT NO. 1

Nuclear Data 3300 Pulse Height Analyzer system. The resulting data were read out on magnetic tape for retention. Printout of this data by a IBM 7040 computer and plots obtained from the analyzer via an Omnigraph X-Y recorder were subsequently used to analyse the spectra.

2.3 Detector Properties

(a) Resolution

While Ge(Li) detectors exhibit considerably less photo-efficiency than NaI(Tl) counters, as seen in the next section, their greatly improved resolution more than compensates for their inefficiency. The best resolution one might possibly expect from a 3"x3" NaI(Tl) detector is about 6% (full width at half maximum of peak) while the resolution for this particular Ge(Li) detector at the time of the experiment varied from about 6 keV at 0.8 Mev to about 15 keV at 7.8 Mev (0.75% and 0.2% respectively).

The above resolution figures given for this detector are about a factor of two worse than when the counter was originally fabricated. The loss of resolution is suggestive of radiation damage produced by fast neutrons. The interaction of fast neutrons with the counter can be inferred by the presence of the 696-keV "gamma-ray" peak seen in typical spectra (see for example Fig. 3-2). This peak corresponds to the de-excitation of the first state in Ge. Since this state has spin 0 decay proceeds through electron conversion. The skew of the peak to the high energy side arises from the addition of the nuclear recoil energy to the electron energy. Another indication of this deterioration was the very poor photopeak to compton peak height ratios. For the sum

of the ^{27}Al (n, n', γ) ^{27}Al runs the ratio for the 1014 keV γ-ray was about 3:2 while the expected (and originally attainable) ratio for this energy and counter size should be better than 5:1 (4).

(b) Efficiency

Solid state Ge(Li) detectors are considerably less efficient than NaI(Tl) as can be seen in (4) but, as mentioned in the previous section, this is more than compensated for by the large improvement in resolution.

Figure 2-3 exhibits the relative efficiency vs γ-ray energy curves for both photopeak heights and double escape peak heights for the present detector as determined by using well-known intensity standards. This curve was then used to calculate the relative intensities of the various γ-rays in the observed spectra.

As can be seen from Figure 2-3 the main contributions to the spectrum above 2.5 Mev are from the double escape peaks. In fact, above about 4.0 Mev the photopeaks are seldom observable. In this region the photoelectric crossection is very low with respect to the pair production crossection. Since the photoelectric crossection drops so rapid with energy for these detectors there is a region between about 1.5 to 2.5 Mev where both the above crossections are very low. As a result γ-rays peaks in this region show up with relative inefficiency compared to the regions below this where the photopeaks predominate and that above where the double escape peaks predominate. This property sometimes leads to difficulties in using the Ge(Li) detectors for low intensity γ-rays in this region.

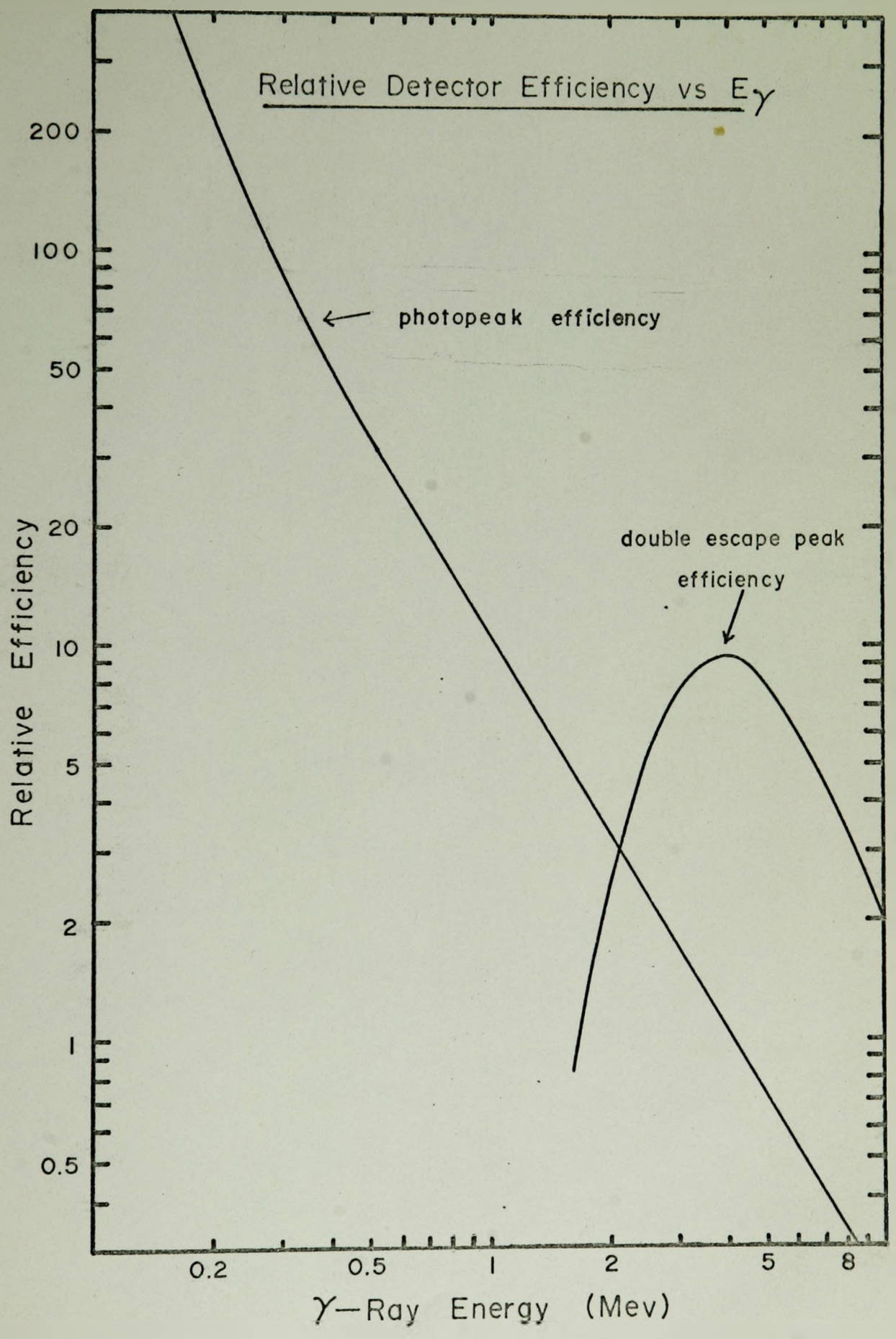
Relative Detector Efficiency vs Eγ
photopeak efficiency
double escape peak efficiency
Relative Efficiency
200
100
50
20
10
5
2
1
0.5
0.2
0.5
1
2
5
8
γ—Ray Energy (Mev)

FIGURE 2-3

(c) Energy Calibration

The detector, as such, was not calibrated for energy response in terms of output pulse height vs γ-ray energy. Instead, the whole data collection system was calibrated in terms of analyzer channel number vs γ-ray energy as will be described later. This allows one to compensate in one step for all the non-linearities of the detector, pulse amplifier and analogue to digital convertor.

2.4 Neutron Beam

(a) Thermal Neutron Flux Reduction

Since the beam port used was originally designed to extract a thermal neutron flux with a minimum of fast neutrons it was necessary to completely reverse the roll of the facility. Removal of some of the quartz filters results in a much increased transmission of fast neutrons. Insertion of a boron-polyethylene shutter greatly reduced the thermal neutron component and produced little change in the fast neutron component. The effect of this shutter was determined in the following way.

By comparing the peak heights of a (n, n', γ) line and a (n, γ) line in both a run with the shutter open and a run with it closed, one can set a lower limit on the value of the thermal neutron flux reduction with respect to the fast neutron flux.

To enable this to be done unambiguously a combination of lines was needed whereby there would not be any interference in either run by nearby lines. Likewise it was necessary to use lines from an element whose most abundant stable isotope, ${}^{A}_{Z}X_{N}$, was such that isotope

$^{A+1}_{Z}Y_{N+1}$ was not stable. For the range of elements in the present investigation there are three such isotopes, $^{27}_{13}Al_{14}$, $^{31}_{15}P_{16}$ and $^{35}_{17}Cl_{18}$.

With ^{27}Al one can use the 843 keV γ-ray arising from the (n, n', γ) reaction and the 1779 keV γ-ray from the β, γ decay of (n, γ) produced ^{28}Al. In this case one opens the shutter approximately 10 minutes before starting acquisition of data during the shutter open run to allow the 2.3 minute ^{28}Al to reach saturation. Likewise one makes sure that the shutter has been closed at least 10 minutes before acquiring a shutter closed spectrum although in this case it is not quite so important as the runs are long compared with the half life of ^{28}Al.

The shutter open run produced relative peak heights of 2640 ± 60 counts and 390 ± 53 counts for the 1779 keV and 843 keV. γ-ray peaks respectively. The relative peak heights for the shutter closed runs were 275 ± 67 counts and 18800 ± 180 counts respectively. Normalizing these results using the 843 keV peak one sees that the equivalent 1779 keV peak height in the first case is 127,261 counts compared to 275 counts in the second case. This results in a thermal flux reduction factor relative to the fast neutron flux of approximately 465 between the shutter open and the shutter closed runs. However, as there is a considerable amount of aluminum in the beam port structure, these results are not entirely unambiguous but represent only the lower limit of the value of the reduction factor with a more probable value somewhat higher.

The ^{35}Cl isotope allows one to check the thermal flux reduction factor without the above mentioned complications as there is very little

chlorine, elemental or compounded, about other than that of the target itself. For this determination the γ-rays used are the 787 keV γ-ray peak from the (n, γ) reaction and the 1220 keV γ-ray peak from the (n, n', γ) reaction. The respective peak heights with the shutter open were 1692 ± 55 counts and 50 ± 30 counts while the results with the shutter closed were 275 ± 165 counts and 4967 ± 140 counts, again, respectively. This produces a relative thermal flux reduction factor of ~ 600.

The 636 keV γ-ray arising from the (n, γ) reaction and the 1265 keV γ-ray from the (n, n', γ) reaction allow a similar calculation from the phosphorus data. The shutter open run yield gave heights of 11300 ± 160 in the 636 keV peak and 4465 ± 100 counts in the 1265 keV peak. With the shutter closed the results for the respective peaks were 435 ± 130 and 9780 ± 115 counts. Again normalizing to the (n, n', γ) peak one gets a relative thermal flux reduction factor of ~ 570. This value supports the factor calculated from the chlorine data and confirms our suspicions of the results from the aluminum data.

The phosphorus data also allowed one to check on the absolute reduction factor for the fast flux due to closing the shutter. By correcting data from a (n, γ) run and a (n, n', γ) run for dead time losses (40% and 2-4% respectively) and knowing the respective length of time of each run one finds that there was no appreciable reduction in the fast neutron flux by closing the shutter.

The above calculations and arguments lead one to the conclusion that closing the shutter reduces the thermal neutron flux with respect to the fast neutron flux by a factor of about 600 without adversely

affecting the fast neutron flux.

(b) Flux Estimate

By using data from Johns and Hughes (3) and (5) one can calculate a very rough estimate of the neutron fluxes involved. The answers arrived at for the shutter closed condition are a thermal neutron flux of $\sim 10^4 n/cm^2/sec$ and a fast neutron flux of $10^6 n/cm^2/sec$.

2.5 Data Acquisition and Analysis

(a) Acquisition

To obtain the inelastic scattering data for each element a series of three or four runs was carried out with the shutter closed. These runs were from two to twenty-four hours in duration with the total running time for each element varying from 18.5 to 40.5 hours. An additional short run with the shutter open was carried out for each element to provide a means of calibrating the spectra using well-known capture γ-ray energies. This was, however, only an approximate calibration as one shall see later.

Since the ND3300 analyzer system had a total memory capacity of 16384 channels one was able to store up to four 4096 channel runs at a time. By using a gain of ~ 2 keV/channel one was able to cover the energy region, up to ~ 8 Mev. As mentioned previously the individual runs for each element were then stored on magnetic tape for printout by computer. Direct addition of these runs was performed in the analyzer and this sum run also put on to magnetic tape. Plots of this sum run and the thermal calibration run were then obtained using the X-Y plotter mentioned in section II-2.

TABLE II-2

EFFECTS OF SUMMING THE INELASTIC SCATTERING RUNS

Run No.	Run Length (Hours)	511 keV Peak			7646" - 7632" keV Peak		
		Channel No.	Peak Height (counts)	Resolution (keV)	Channel No.	Peak Height (counts)	Resolution (keV)
Aluminum runs							
1	5.5	415.5	27000	5.8	3271.5	65	30
2	2.0	414.9	17300	5.4	3268.5	40	23.5
3	11.0	415.1	60000	5.6	3270.4	170	26
SUM	18.5	415.0	101000	5.3	3270.5	270	27
Sulphur runs							
1	4	412.7	11000		3262.8	75	
2	6	412.1	19000		3260.5	120	
3	10	411.6	30000		3257.0	170	
4	1.5	410.9	3900		3256.0	24	
SUM	21.5	411.8	60000	6.0	3258.8	330	14

(b) Gain Shift

Once the data was collected the inelastic scattering runs for each element were compared with one another for gain and zero shift. In all cases there appeared to be no appreciable zero shift and the gain shifts involved were of the order of 3 to 5 channels in 3200 as determined using the 511 keV annihilation γ-ray and the distinctive double escape peaks from the ^{57}Fe doublet at 7632-7646 keV. As there

was one predominantly long run in each set the addition of the other runs to it without correcting for gain shift did not appreciably deteriorate the resolution obtained but did improve the statistical quality of the spectra. Examples of this determination are shown in Table II-2 for the aluminum and sulphur runs. If there was doubt as to smearing of closely spaced peaks a close look was taken at one of the shorter runs. Following this examination, one has a single composite (n, n', γ) spectrum and a (n, γ) spectrum for each element.

(c) Energy Determination

The first step in obtaining the energies of the various peaks was to determine the overall energy/channel value between the 511 keV peak and the double escape peak from the ^{57}Fe doublet, both of which are quite distinctive in (n, n', γ) spectra obtained at this beam port. This value was then used to obtain a first estimate of the energies of the major peaks in the spectrum. The (n, γ) spectrum was also checked to get a first estimate of major peak energies using the above energy/channel value. Once these peaks in the (n, γ) spectrum were definitely identified the most recent energies for these peaks were assigned to the peaks. These plus the 1022 keV differences between photopeaks and double escape peaks were then used to check the energy/channel value for various regions of the spectrum. It was found that this varied from about 2.100 keV/channel at the low end to around 2.150 keV/channel at around 6 Mev. Response of this sort has already been pointed out by Lyoklama et al (6) and is mainly due to non-linear response of the electronic system. At this

point it was noted that the energy/channel value for the (n, γ) runs was slightly different than that necessary to fit certain well-known background peaks in the inelastic spectrum. This was probably due to gain shift as a result of the much higher counting rates associated with the (n, γ) runs than that with the (n, n', γ) runs (40% dead time vs 2-4% dead time, respectively). For these reasons the (n, γ) runs were used mainly for spotting (n, γ) information within the (n, n', γ) spectra rather than for energy calibration.

TABLE II-3

BACKGROUND PEAKS USED IN CALIBRATION

Peak energy (keV)	γ-ray (keV)	Origin
511	511	Annihilation quanta
1294	1293.8	$^{41}A\ (\beta,\gamma)\ ^{41}K$
4898	5920	$^{56}Fe(n, \gamma)\ ^{57}Fe$ double escape
4996	6018	$^{56}Fe(n, \gamma)\ ^{57}Fe$ double escape
6617	7639	7632-7646 doublet from above

The next energy estimate for the major (n, n', γ) peaks was then made on the basis of several well-known background peaks normally present in the spectra and noted in Table II-3. To ensure that these peaks were in fact background peaks the overnight inelastic scattering runs for each of the elements were plotted and the peaks compared as to size, shape and location. This showed up several other background peaks as

noted in Table III-2 but these were either of such a size or shape that they could not be used for accurate energy determination or else other peaks interfered with them.

In the region around 1 to 2 Mev it was usually possible to find a prominant photopeak - double escape peak pair from which one can obtain the energy/channel value. This was then used in conjunction with the 1294 keV ^{41}K peak to fix the energy of these peaks. Another energy/channel value based on the above peak energies was then calculated for use between about 1 Mev and the 511 keV peak. Likewise a third value was obtained from approximately 2 Mev to 5 Mev and another from 5 Mev up using the 4996 keV and 6617 keV peaks. These energy/channel values were then used in their respective regions to assign energy values to all peaks in the spectrum.

Following the assignment of peak energies, the peak heights above background were recorded along with their estimated errors as in the following formula

$$\text{Peak height} = N-B \pm \sqrt{N+B} \qquad (2.1)$$

where N is the recorded counts in the channel containing the peak top and B is the background count under the peak. The obvious photopeaks were noted along with their double escape peaks where applicable and checked against a photopeak height to double escape peak height ratio vs γ-ray energy curve for consistency. Single escape peaks were noticed only for a few very intense peaks in the spectrum, provided they were not obscured in or by other peaks. In some cases the above check led to discovery of a double escape peak included in a photopeak and vice-versa, depending from which direction one approached this.

This was an iterative process in some instances where the decay scheme analysis led to a rechecking of intensities.

(d) Decay Scheme Determinations

Using the previously determined peak heights and the relative efficiency curves of Figure 2-3 the relative intensities of the γ-rays were determined from the following formula.

$$RI_i = \frac{RH_i}{RE_i} \qquad (2.2)$$

where RI_i, RH_i and RE_i are the Relative Intensity, Relative Peak height and Relative Efficiency for the ith peak. This would allow one to compare the branching ratios of γ-rays from levels exhibiting multiple paths of de-excitation.

With the γ-ray energies and their relative intensities now known the decay scheme, including branching ratios, was constructed using the data of Endt et al (7)(8) as a guide. After some reiterative procedures a decay scheme was constructed for each isotope involved. To facilitate this a check was made on the γ-ray requirements for the competing neutron reactions (n, α) (n,p) and (n,d). In each case several of the previously unaccounted for γ-ray energies were given assignments.

(e) Primary Population of Nuclear Levels

The relative number of γ-rays arising out of the (n, n') population of each nuclear level was then determined by subtracting the relative number of γ-rays entering the level from the number de-exciting the level. The resulting relative population values were then treated in two ways.

The first approach was to plot the relative population values vs the energy of the level involved on semi-logarithmic paper and attempt straight line fits between levels of the same spin and parity assignment. For the even-even nuclides involved these curves were compared with those generated using Feshbach's theory (1) as presented in the introduction.

The second method was to correct the relative population values for the crossection and flux distribution changes with energy using the method of Donahue (2) as mentioned in the introduction. In this case the values used for the parameters α and β were 0.6 Mev^{-1} and 3 Mev^{-1} as determined from (5). These results were then plotted as corrected relative population values vs the energy of the level involved along with notation of their spin and parity assignment as given by (7) and (8).

CHAPTER III

RESULTS AND DISCUSSION

3.1 General

Since, in many cases, the types of arguments and discussion are the same for each of the five elements investigated one can examine one in detail to show the application of the methods previously described and then present the results of the rest, noting any irregularities, without losing any of their intrinsic value. Based on this premise one can proceed to present and evaluate the $^{27}Al\ (n, n', \gamma)\ ^{27}Al$ reaction results in detail, followed by the presentation of the remaining nuclides.

3.2 Aluminum $^{27}Al(n, n', \gamma)\ ^{27}Al$

(a) γ-ray Energy Determinations

The composite sum spectrum for the inelastic neutron scattering runs for aluminum is shown in Figure 3-1. As naturally occuring aluminum is monoisotopic the main peaks in this spectrum, other than background peaks, will be associated with the de-excitation of the nuclear energy levels of $^{27}_{13}Al_{14}$.

The initial calibration figure using the annihilation quanta and ^{57}Fe doublet peaks as mentioned in Section 2.5 (c) was 2.138 keV per channel. The resulting energy assignments for the major peaks using this value were as shown in Table III-1.

From similar investigations of the other spectra it was determined that peaks 6 and 7 of Table III-1 were the double escape peaks from

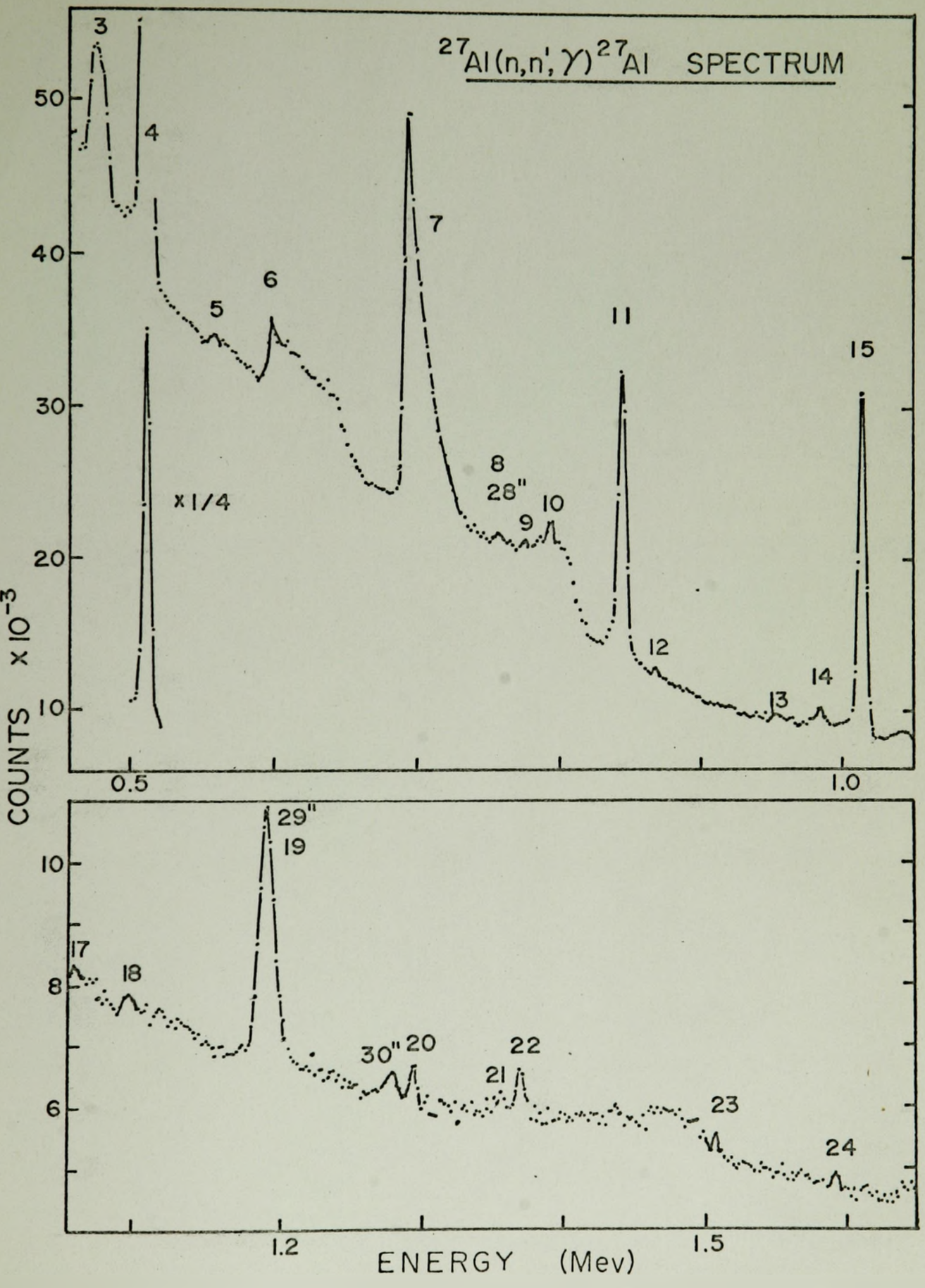
$^{27}Al(n,n',\gamma)^{27}Al$ SPECTRUM
COUNTS x 10^{-3}
x 1/4
ENERGY (Mev)
0.5
1.0
1.2
1.5
3
4
5
6
7
8
28"
9
10
11
12
13
14
15
17
18
29"
19
30"
20
21
22
23
24

FIGURE 3-1 (a)

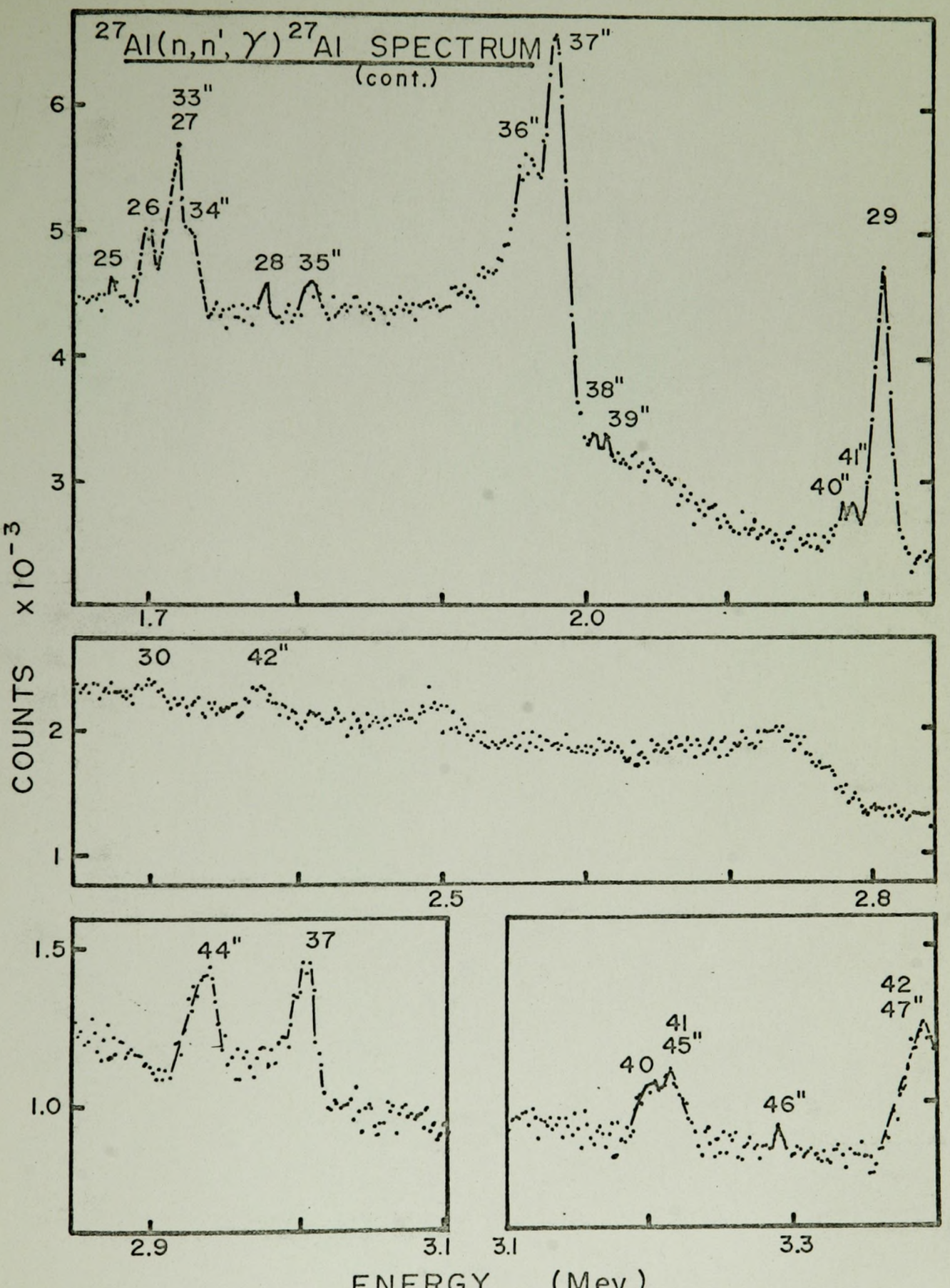
$^{27}Al(n,n',\gamma)^{27}Al$ SPECTRUM (cont.)
COUNTS x 10^{-3}
ENERGY (Mev)
25
26
27
33"
34"
28
35"
36"
37"
38"
39"
40"
41"
29
30
42"
44"
37
40
41
45"
46"
42
47"
1.7
2.0
2.5
2.8
2.9
3.1
3.3

FIGURE 3-1(b)

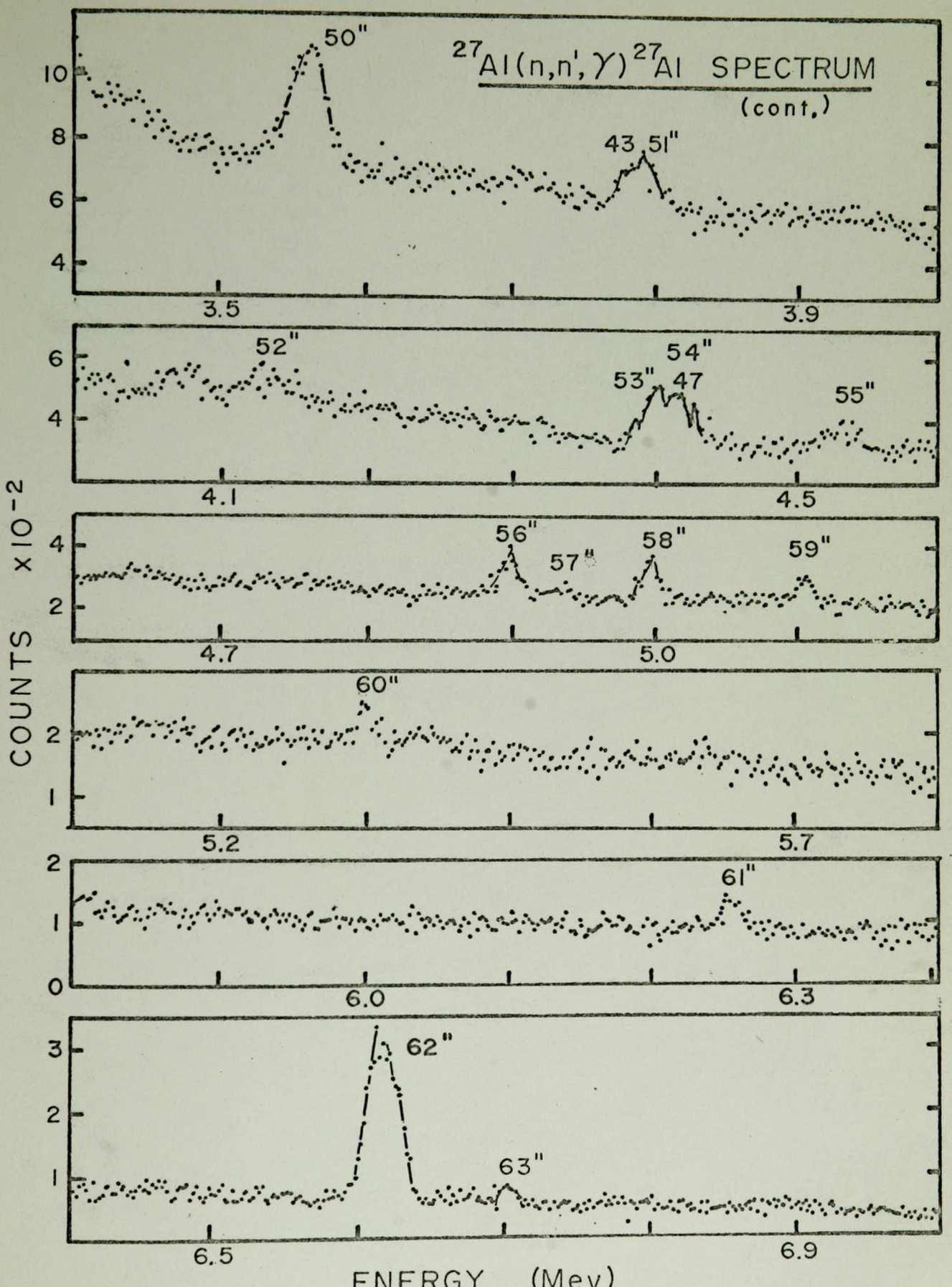
$^{27}Al(n,n',\gamma)^{27}Al$ SPECTRUM
(cont.)
50"
43
51"
52"
53"
54"
47
55"
56"
57"
58"
59"
60"
61"
62"
63"
COUNTS X10-2
ENERGY (Mev)
3.5
3.9
4.1
4.5
4.7
5.0
5.2
5.7
6.0
6.3
6.5
6.9

FIGURE 3—1(c)

TABLE III-1

ENERGY CALIBRATION OF $^{27}Al(n, n', \gamma)\ ^{27}Al$ PEAKS

Peak No.+	Channel No.	Using 2.138 keV /Channel	Using Endt et al(8)	Using ^{41}A & ^{24}Na decay lines	Final calibration lines
1	415	*511	* 511	* 511	511
2	572	847	* 843	843	843.5
3	652.5	1019	*1013	1014	1014
4	734.7	1195	1188	1190	1190
5	1214	2219	*2209	2212	2212
6	2470	4905	*4898	*4898	4898
7	2516	5003	*4996	*4996	4996
8	3270.5	*6617	*6617	*6617	6617
9	783.5		1292	*1294	1294
10	818.4		1366.4	*1368.5	1368.5
11	989		1730	*1732	1732

* energies used for this calibration

+ these peak numbers bear no relationship to those used in Table III-2 and Figure 3-1.

the 5920 and 6018 keV γ-rays of ^{57}Fe. As mentioned in Section 2.5 (c) these peaks, along with the double escape peak from the 6130 keV ^{16}N (β,γ) ^{16}O decay γ-ray, were quite noticeable in all of the inelastic scattering spectra. The new values given by Endt et al (8) for the first three levels of ^{27}Al were then assigned to peaks 2, 3 and 5 of Table III-1 with the resulting calculated peak energies as shown.

It was then noted that the energy assignment of the ^{41}A decay line (1293.8 keV) (#9 in Table III-1) which appears in all spectra was 2 keV low as were the two accurately known ^{24}Na (β,γ) decay lines (1368.5 and 2753.9" keV) (#10 and #11 in Table III-1) observed from the ^{24}Na (β,γ) ^{24}Mg decay lines from the ^{27}Al (n, α) ^{24}Na reaction. When these were raised to their proper values one obtained the results shown in the next column of Table III-1. In this set of determinations the 1022 keV difference between peaks 4 and 5 was used to establish an energy per channel value for this region which was then coupled with the 1294 keV peak to obtain the energy assignment shown for peak 4. Peak 5 was then set 1022 keV above this. The resulting energy assignments for peaks 10 and 11 confirm the above procedure.

These energies were then checked against recent independent work on the ^{27}Al (n, γ) ^{28}Al reaction done by Nichol et al (9) in which the prominent ^{27}Al (n, n', γ) ^{27}Al peaks were seen. This work confirmed the energy assignments for peaks 3, 4 and 5 of the table and resulted in the assignment of 843.5 keV to peak 2. The energies shown in the last column of Table III-1 were then used to work out the

peak energies for the remaining peaks of the spectrum. The resulting γ-rays energies were as listed in Table III-2.

(b) Decay Scheme

The next step was to establish the peak heights for relative intensity correction calculations. During this process the known photopeak to double escape peak height ratios were checked and verified. At the same time the γ-ray assignments in the decay scheme were made in a sort of iterative process of assignment, checking and verification as mentioned in Section 2.5 (d) using the data from Endt et al (7) (8) and (10).

In the case of the 2212 keV double escape peak it was found that there must be a photopeak included in it. This was later assigned to the 2212 - 1014 keV transition. This same technique was applied to the double escape peak for the 1780 keV γ-ray to expose another photopeak. To separate the photopeak of the 4409 keV γ-ray from the double escape peak of the 5434 keV γ-ray , the procedure was applied in reverse.

The γ-ray energies associated with the following competing neutron reactions

$$^{27}Al\ (n,\ \alpha\ ,\ \gamma)\ ^{24}Na\ (\beta^-,\ \gamma)\ ^{24}Mg$$

$$^{27}Al\ (n,\ p\ ,\ \gamma)\ ^{27}Mg\ (\beta^-,\ \gamma)\ ^{27}Al$$

$$^{27}Al\ (n,\ d,\ \gamma)\ ^{26}Mg$$

were also checked against the present list of γ-rays. Additional consistant evidence of the previously noted (n,α) reaction was found in the presence of the 868.5 keV γ-ray which is the approximate de-excitation energy of the 1341 keV level of ^{24}Na. The 984 keV and

TABLE III-2

γ-RAYS FROM $^{27}Al(n, n', \gamma)\ ^{27}Al$ REACTION

Line No.	Energy* (Error)	Relative Intensity (Error)	Assignment
1	171 (3)	75 (3)	1014-843.5
2	197 (3)		Background, ^{75}Ge
3	477 (3)		Background, ^{10}B
4	511		Annihilation
5	560 (3)		Background
6	598 (3)		Background, $^{74}Ge(n,n',\gamma)$
7	696 (3)		Background, $^{72}Ge(n,n',\gamma)$
8	756 (4)	30 (19)	4811-4053 + ?
9	775 (3)	25 (10)	?
10	792 (3)	90 (13)	3004-2212
11	843.5(3)	1392 (18)	843.5-0
12	868.5(3)	42 (8)	$^{27}Al(n,\alpha)^{24}Na$+Background
13	955 (3)	31 (9)	$^{27}Al(n,p)^{27}Mg$
14	984 (3)	112 (10)	$^{27}Al(n,p)^{27}Mg$
15	1014 (3)	2180 (20)	1014-0
16	1042 (5)	49 (10)	Background
17	1055 (2)	43 (9)	Background
18	1095 (4)	36 (10)	Background, $^{58}Fe(n,\gamma)^{59}Fe$
19	1190 (6)	170 (39)	?
	(1198)	15	2212-1014
20	1294 (3)	103 (15)	Background, $^{41}A(\beta,\gamma)^{41}K$
21	1355 (4)	55 (12)	Background
22	1368.5 (2)	40 (25)	2212-843.5
	1368.5 (2)	80 (11)	$^{24}Na(\beta,\gamma)^{24}Mg$
23	1506 (1)	56 (14)	4511-3004
24	1591 (2)	52 (15)	Background
25	1676 (3)	40 (16)	Background

TABLE III-2 (cont'd.)

γ-RAYS FROM $^{27}Al(n, n', \gamma)\ ^{27}Al$ REACTION

Line No.	Energy* (Error)	Relative Intensity (Error)	Assignment
26	1701 (5)	126 (15)	$2212' + {}^{27}Al(n,p)^{27}Mg$
27	1721 (6)	310 (20)	2734.5-1014
28	1780 (3)	62 (16)	$^{28}Al(\beta, \gamma)^{28}Si$
29	2212 (5)	840 (35)	2212-0
30	2300 (5)	86 (10)	4511-2212
31	2602 (4)	14 (12)	4814-2212
32	2665 (3)	42 (2)	3679-1014
33	2735 (4)	81 (17)	2734.5-0
34	2754 (4)	80 (11)	$^{24}Na(\beta,\gamma)^{24}Mg$
35	2835 (5)	41 (10)	3679-843.5
36	2984 (4)	50 (30)	2984-0
37	3004 (4)	250 (15)	3004-0
38	3038 (3)	53 (18)	5250-2212
39	3045 (3)	28 (18)	4056-1014
40	3203 (3)	19 (8)	5412-2212
41	3211 (4)	31 (8)	4056-843.5
42	3396.5 (4)	23 (6)	4410.5-1014
43	(3798)		4814-1014
44	3957 (6)	35 (4)	3957-0
45	4236 (8)	19 (5)	5250-1014
46	4312 (4)	11 (4)	5155-843.5
47	4410.5 (6)	44 (7)	4410.5-0
48	4430 (20)		^{12}C
49	4512 (3)	6 (3)	4511-0
50	4582 (10)	43 (4)	4582-0

TABLE III-2 (cont'd.)

γ-RAYS FROM $^{27}Al(n, n', \gamma)\ ^{27}Al$ REACTION

Line No.	Energy* (Error)	Relative Intensity (Error)	Assignment
51	4811 (12)	18 (3)	4814-0
52	5155 (10)	11 (3)	5155-0
53	5409 (3)	7 (3)	5412-0
54	5434 (6)	9 (5)	5434-0
55	5556 (4)	22 (3)	5556-0
56	5920 (6)	23 (3)	Background, Fe(n, γ)
57	5955 (2)	8 (3)	5955-0
58	6018 (4)	23 (6)	Background, Fe(n, γ)
59	6128 (4)	14 (6)	Background, $^{16}N(\beta,\gamma)^{16}O$
60	6420		Background
61	7275		Background, ^{57}Fe
62	7632		Backgroumd, $^{56}Fe(n,\gamma)^{57}Fe$
	7646		Background $^{56}Fe(n,\gamma)^{57}Fe$
63	7724		Background, ?
64	9298		Background, $^{54}Fe(n,\gamma)^{55}Fe$

* All energies are in keV.

γ-ray energies in brackets are energies assumed from other requirements.

and 953 keV γ-rays are evidence along with part of the 1701 peak of the (n, p) reaction. They represent the de-excitation γ's of the first three levels of ^{27}Mg (8). There was no obvious evidence of the (n, d) reaction. It might be noted at this point that the check on the relative intensities of the ^{24}Na (β,γ) decay lines revealed the 1368.5 keV transition from the 2212-843.5 keV levels.

A decay scheme for ^{27}Al was then plotted as shown in Figure 3-2. The de-excitation γ-rays from each level were then checked against Endt et al (7) (8) and Mathur et al (11) for branching ratio consistency. Where it was possible that a low intensity γ-ray called for was hidden in or by another high intensity peak it was added to the decay scheme as a dashed transition (namely the 2212-1014, 4410.5-2212, 4511-2734.5 transitions which were hidden in the 2212", 2212 and 1780 peaks respectively). The 3798 keV line from the 4814-1014 transition was called for but not observed. The 756 keV γ-ray (or at least part of it) could be a transition from the 4814 keV to the 4056 keV level but would have to be confirmed by coincidence experiments.

A summary of this branching ratio data along with a comparison with previous results is shown in Table III-3. On the whole there is good agreement with Endt et al (8). The notable exceptions are the de-excitation of the 4814 keV level, as mentioned previously, and that of the 5250 keV level where the present work and the reference seem to be in opposition.

Once the above procedures were ended one has a table of γ-rays with their energies, relative intensities and assignments as given

^{27}Al DECAY SCHEME

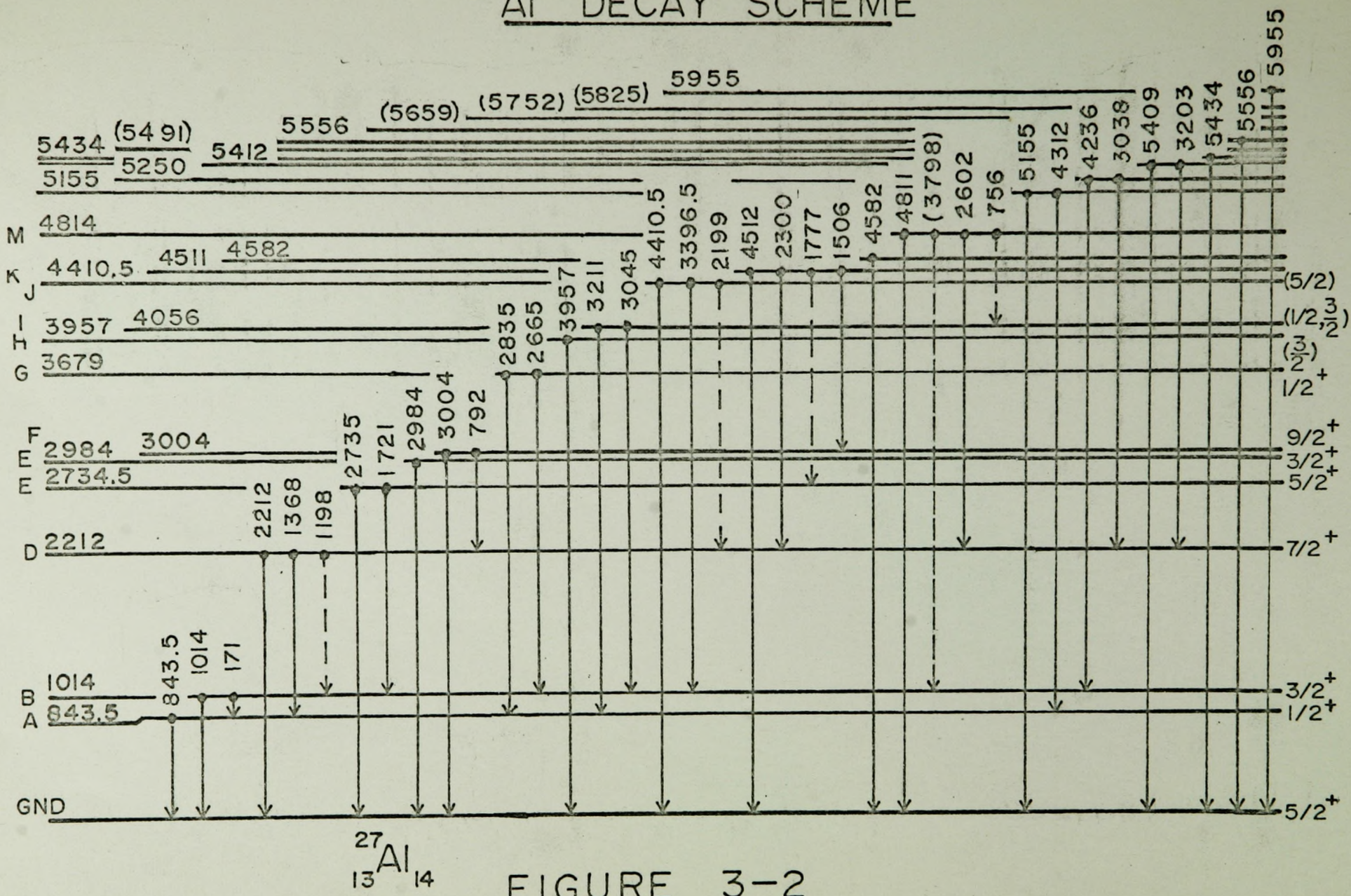

$^{27}_{13}Al_{14}$

FIGURE 3-2

TABLE III-3

^{27}Al BRANCHING RATIOS

Energy Level	Present Work			Endt et al (8)	Endt et al (7)	Mathur et al (11)
	Level Energy	Decay γ-rays	Branching Ratio			
A	843.5 (3)	843.5 (3)	100	100	100	100
B	1014 (3)	1014 (3)	97 (1)	97	98	98
		170.5 (2)	3 (0.5)	3	2	2
C	2212 (4)	2212 (4)	94 (4)	100	100	100
		1368.5 (2)	4 (3)		<2	
		(1198)	1.6		<2	
D	2734.5 (4)	2735 (4)	21 (4)	24	10	~25
		1721 (6)	79 (5)	76	>90	~75
E	2984 (4)	2984 (4)	100	99	+	p
				1	+	
F	3004 (4)	3004 (4)	74 (4)	87	3000	~84
		792 (3)	26 (4)	13	+	~16
					+	p
					+	p
G	3679 (2)	2835 (5)	49 (12)	65	p	p
		2665 (3)	51 (14)	35		
H	3957 (6)	3957 (6)	100	100		
I	4056 (6)	3211 (4)	53 (27)	80	p	p
		3045 (3)	47 (31)	20		
J	4410.5 (6)	4410.5 (6)	53 (8)	55		
		3396.5 (4)	27 (7)	25		
		(2199)	*20	20		
K	4511 (4)	4512 (3)	4 (2)	10		
		2300 (5)	52 (6)	60		
		1506 (2)	34 (9)	20		
		(1777)	*10	10		
L	4582 (10)	4582 (10)	100			
M	4814 (6)	4811 (12)	29 (5)	40		
		2602 (6)	23 (19)	35		
		756[1] (4)	48 (31)			
		(3798)	?	25		

TABLE III-3 (cont'd.)

^{27}Al BRANCHING RATIOS

Energy Level	Present Work			Endt et al (8)	Endt et al (7)	Mathur et al (11)
	Level Energy	Decay γ-rays	Branching Ratio			
M	5155 (6)	5155 (10)	50 (14)			
		4312 (4)	50 (14)			
O	5250 (6)	4236 (8)	26 (7)	70		
		3038 (3)	74 (25)	20		
		(5250)	?	10		
P	5412 (6)	5409 (3)	27 (11)			
		3203 (3)	73 (30)			

* transitions indicated but not assigned to either of the two levels involved

p transitions indicated

* branching ratio and γ-ray energy assumed for hidden peak

? transition called for but not observed

n transition suggested by present work

( ) errors assumed (HWHM)

in Table III-2.

The observed energy levels were then calculated from the present data and compared with previous work as shown in Table III-4. One sees that the present work agrees very well with Endt et al (8) except for the first three levels. The present 2212 keV level, however, does agree with the other three references (7)(9)(11) while the 843.5 and 1014 keV levels are within the estimated errors for references (7) and (9).

Further confirmation was added by comparing these results with previously published (n, n', γ) work by Mathur et al (11) and as found in (10). This comparison is presented in Table III-5. The present work is in agreement, within estimated errors, with all the reported previous work.

(e) Primary Population of Levels

Once the decay scheme was reasonably settled the relative primary population values for each level were calculated as described in Section 2.5 (e). In this case one had to subtract out the contributions to the first two levels from the ^{27}Mg (β, γ) decay from the ^{27}Al(n,p)^{27}Mg reaction.

The decay scheme involved in this calculation as shown in Figure 3-3 was taken from (8). Although the 1936 keV γ-ray was not observed, because of statistics, it was assumed to be there in the proper ratio. Likewise the 1692 keV γ-ray was assumed to be buried in the 2212 keV γ-ray single escape peak (1701 keV). For this determination its intensity was set equal to the assumed total intensity for the decay of the 1936 keV level. Thus the total assumed number

TABLE III-4

LEVEL ENERGIES* OF ^{27}Al

Energy Level	Present Work	Endt et al (8)	Endt et al (7)	Mathur et al (11)	Nichol et al (9)
A	843.5(3)	842.9(0.3)	842.4(1.4)	842	843.5
B	1014 (3)	1013.0(0.3)	1013 (2)	1013	1013.9
C	2212 (4)	2208.9(0.6)	2212 (3)	2212	2212.0
D	2734.5(4)	2732.0(0.8)	2731 (3)	2730(10)	
E	2984 (4)	2979.7(0.9)	2976 (3)	2976	
F	3004 (4)	3000.6(1.0)	3000 (3)	3000(10)	
G	3679 (4)	3677.8(1.0)	3674 (5)		
H	3957 (6)	3955.9(1.3)	3951 (5)		
I	4056 (6)	4054.8(1.4)	4052 (5)		
J	4410.5(6)	4409 (2)	4403 (6)		
K	4511 (4)	4508 (5)	4504 (5)		
L	4582 (10)	4580 (2)	4576 (6)		
M	4814 (6)	4811 (2)	4805 (6)		
N	5155 (6)	5155 (3)	5149 (5)		
O	5250 (6)	5246 (2)	5240 (5)		
P	5412 (6)	5410 (6)	5410 (6)		
Q	5434 (6)	5434 (2)	5424 (5)		
R		5491 (6)	5491 (6)		
S	5556 (4)	5550 (2)	5543 (5)		
T		5659 (6)	5659 (6)		
U		5752 (4)	5745 (12)		
V		5825 (6)	5821 (5)		
W	5955 (2)	5955 (6)	5951 (5)		
X		6082 (2)	6074 (12)		

* All energies in keV

TABLE III-5

COMPARISON WITH PREVIOUS $^{27}Al(n, n', \gamma)$ WORK

Present Work Reactor n.	Mathur et al (11) $E_n < 4.57$*	Data from Nuclear Data Sheets (10) 59M118 $E_n = 2.7$	59H92 $E_n = 2.95$	56D23 $E_n = 2.56$	55G18 $E_n = 4.5$
0.171 (3)	+			0.166(3)	
0.792 (3)	+				
0.8435 (30)	0.84	0.860(20)	0.840(10)	0.840(8)	0.84 (2)
1.014 (3)	1.013	1.035(20)	1.02 (3)	1.017(10)	1.02 (3)
1.721 (6)	1.72				
2.212 (5)	2.21	2.240(30)	2.19 (6)	2.21 (2)	2.27 (6)
2.735 (4)	2.73				
2.835 (5)	+				
2.984 (4)	2.976				
3.004 (4)	3.00				3.10 (8)
3.211 (4)	+				

* All energies are in Mev with errors in least significant figures in brackets

+ Transitions noted but no energy assignment given.

^{27}Mg CONTRIBUTION TO ^{27}Al SPECTRUM

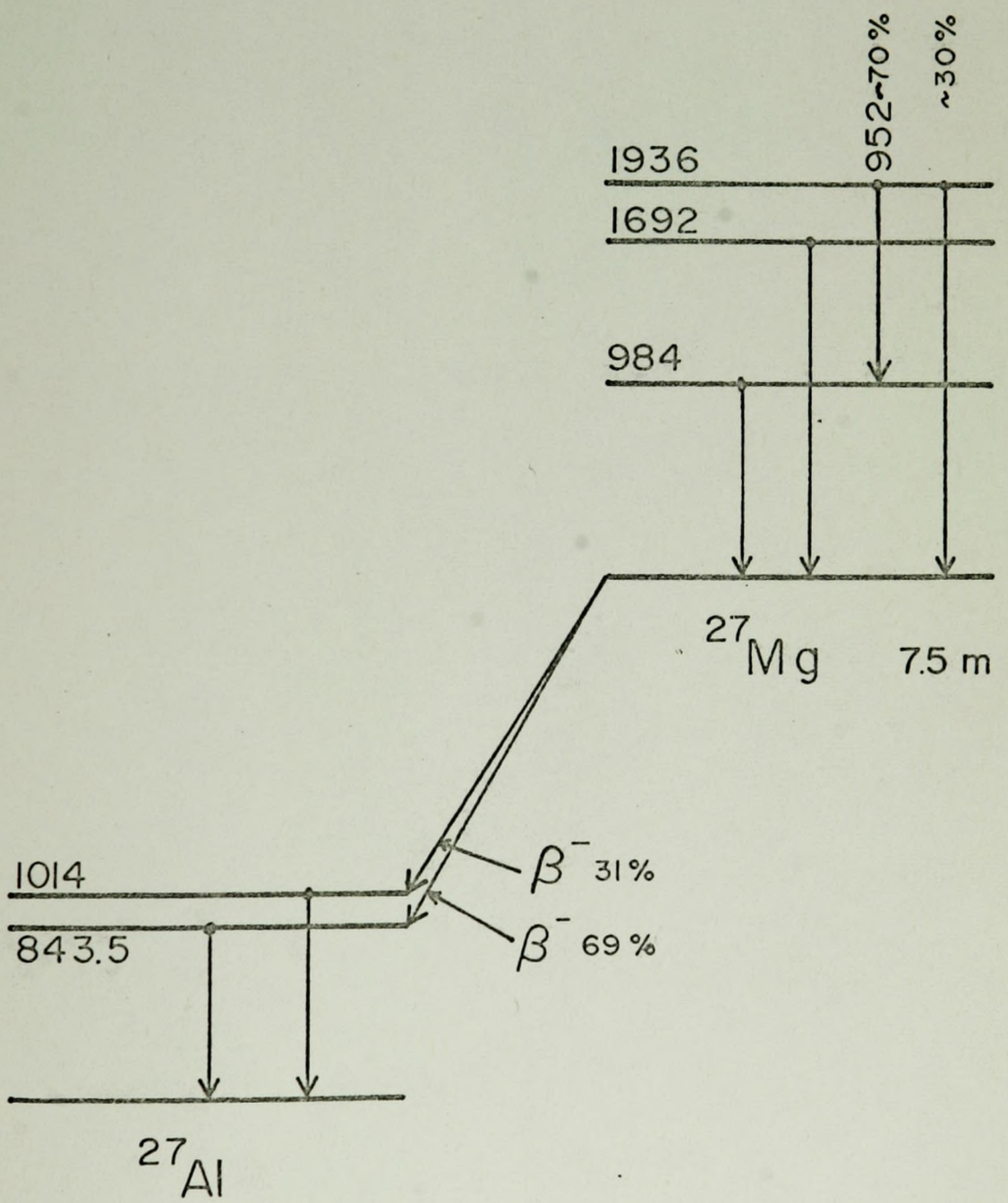

FIGURE 3—3

TABLE III-6

PRIMARY POPULATION VALUES FOR ^{27}Al

Level	Energy	Spin (from (8))	Relative Primary Population Value	Corrected Relative Values	Spins Predicted (Fig. 3-5)
GND	0	$5/2^+$			
A	843.5	$1/2^+$	1076 (85)	1780 (140)	
B	1014	$3/2^+$	1793 (75)	3260 (137)	
C	2212	$7/2^+$	616 (125)	2280 (463)	
D	2734.5	$5/2^+$	374 (43)	1908 (220)	
E	2984	$3/2^+$	50 (30)	298 (180)	
F	3004	$9/2^+$	284 (42)	1711 (253)	
G	3679	$1/2^+$	83 (22)	755 (200)	
H	3957	(3/2)	35 (4)	372 (43)	$3/2^+$
I	4056	(1/2,3/2)	29 (45)	330 (510)	(1/2, 3/2)
J	4410.5	(5/2)	84 (16)	1184 (225)	5/2
K	4511		165 (30)	2465 (448)	$7/2^+$
L	4582		43 (4)	672 (63)	$1/2^+$
M	4814		62 (34)	1106 (687)	$(1/2^+, 5/2^-, 9/2^+)$
N	5155		22 (6)	500 (137)	(1/2, 3/2)
O	5250		72 (23)	1675 (535)	(5/2, 9/2)
P	5412		26 (11)	668 (282)	(1/2)
Q	5434		44 (7)	1158 (184)	$5/2^-$
R	(5491)				
S	5556		22 (5)	612 (139)	$1/2^+$
T	(5659)				
U	(5752)				
V	(5825)				
W	5955		8 (3)	285 (107)	$3/2^+$

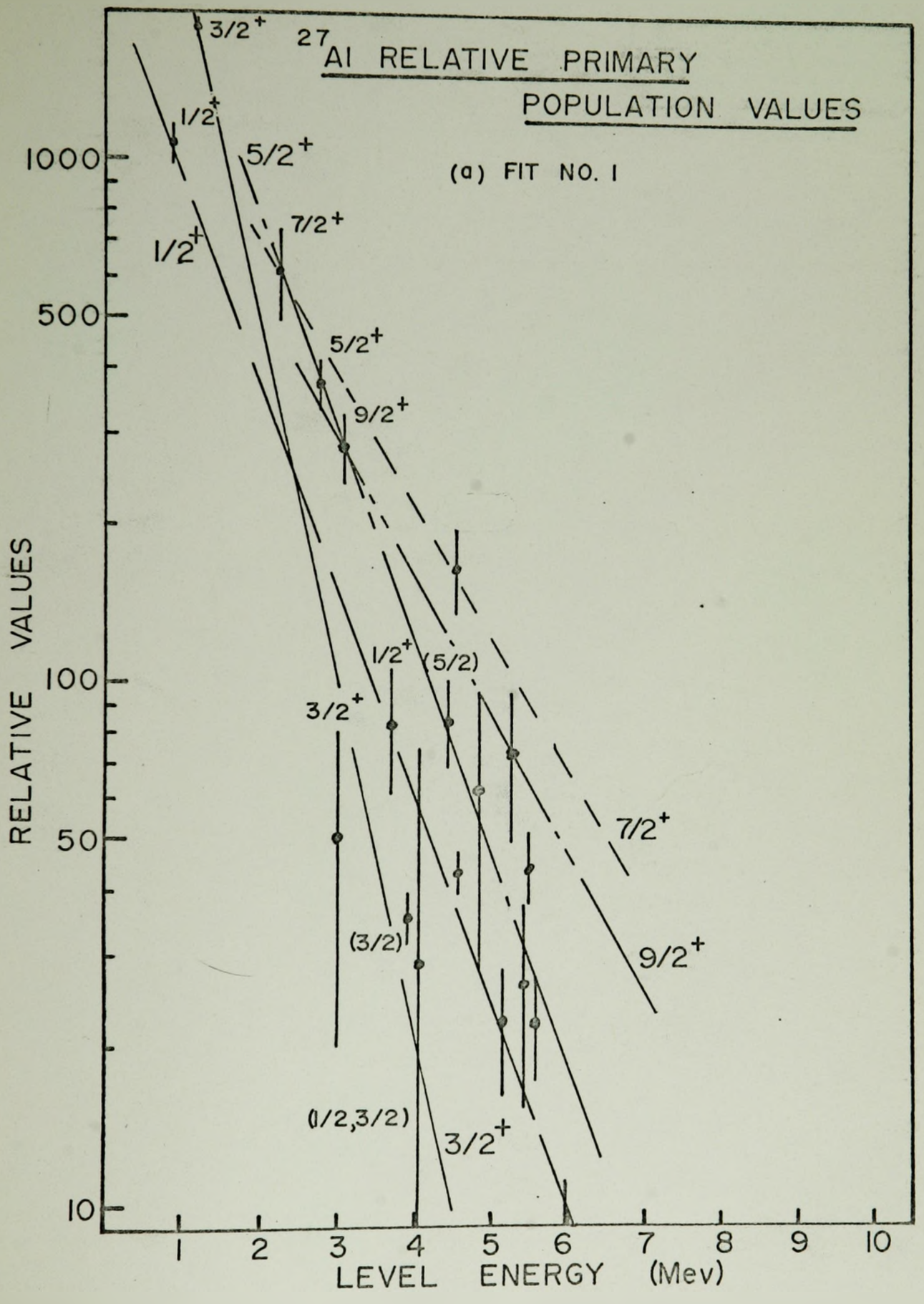
^{27}Al RELATIVE PRIMARY
POPULATION VALUES
(a) FIT NO. 1
3/2+
1/2+
5/2+
7/2+
1/2+
5/2+
9/2+
1/2+
(5/2)
3/2+
7/2+
9/2+
(3/2)
(1/2,3/2)
3/2+
RELATIVE VALUES
1000
500
100
50
10
1
2
3
4
5
6
7
8
9
10
LEVEL ENERGY (Mev)

FIGURE 3-4(a)

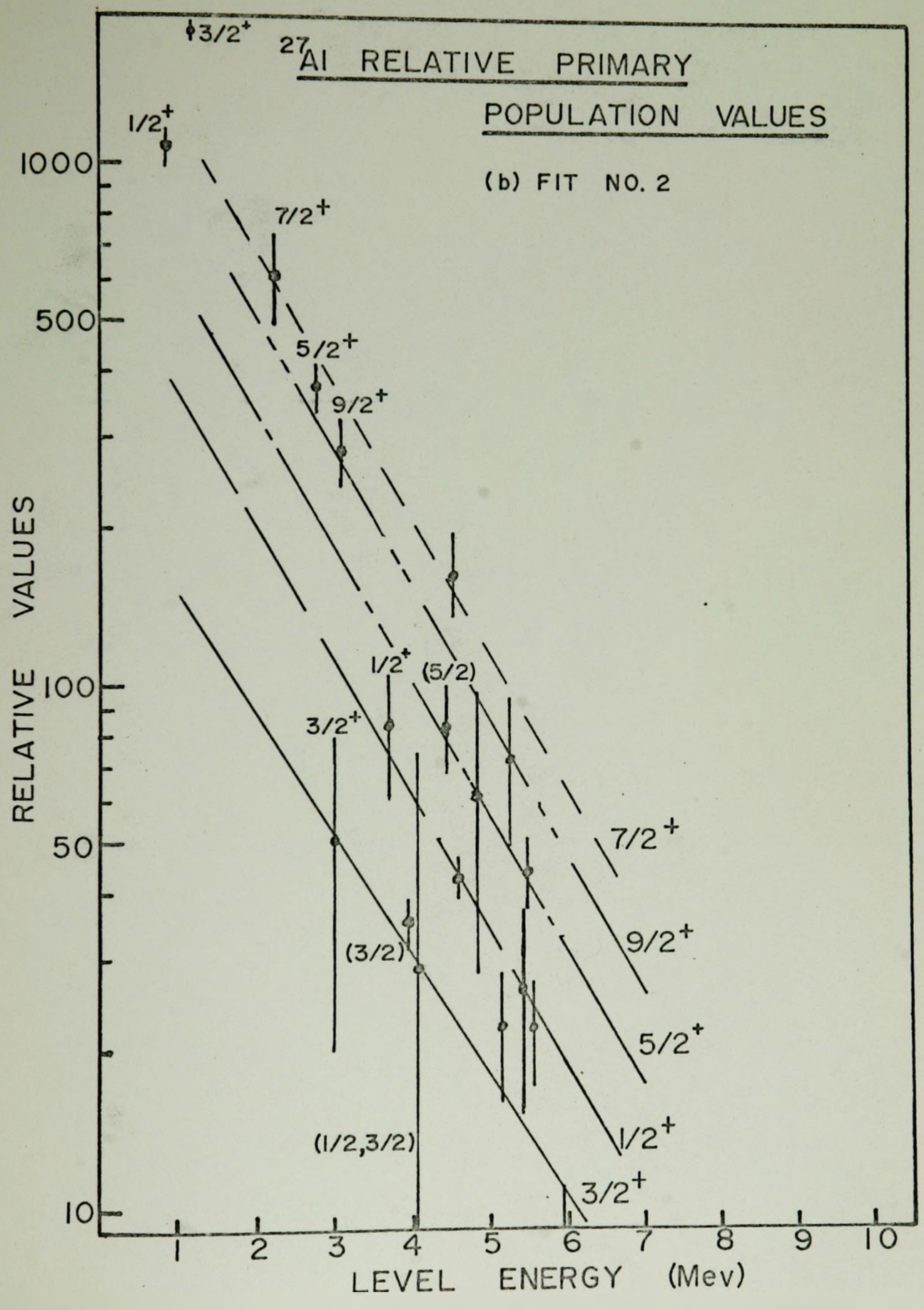
^{27}Al RELATIVE PRIMARY
POPULATION VALUES
(b) FIT NO. 2
3/2+
1/2+
7/2+
5/2+
9/2+
1/2+
(5/2)
3/2+
7/2+
9/2+
5/2+
(3/2)
1/2+
(1/2,3/2)
3/2+
RELATIVE VALUES
1000
500
100
50
10
1
2
3
4
5
6
7
8
9
10
LEVEL ENERGY (Mev)

FIGURE 3-4(b)

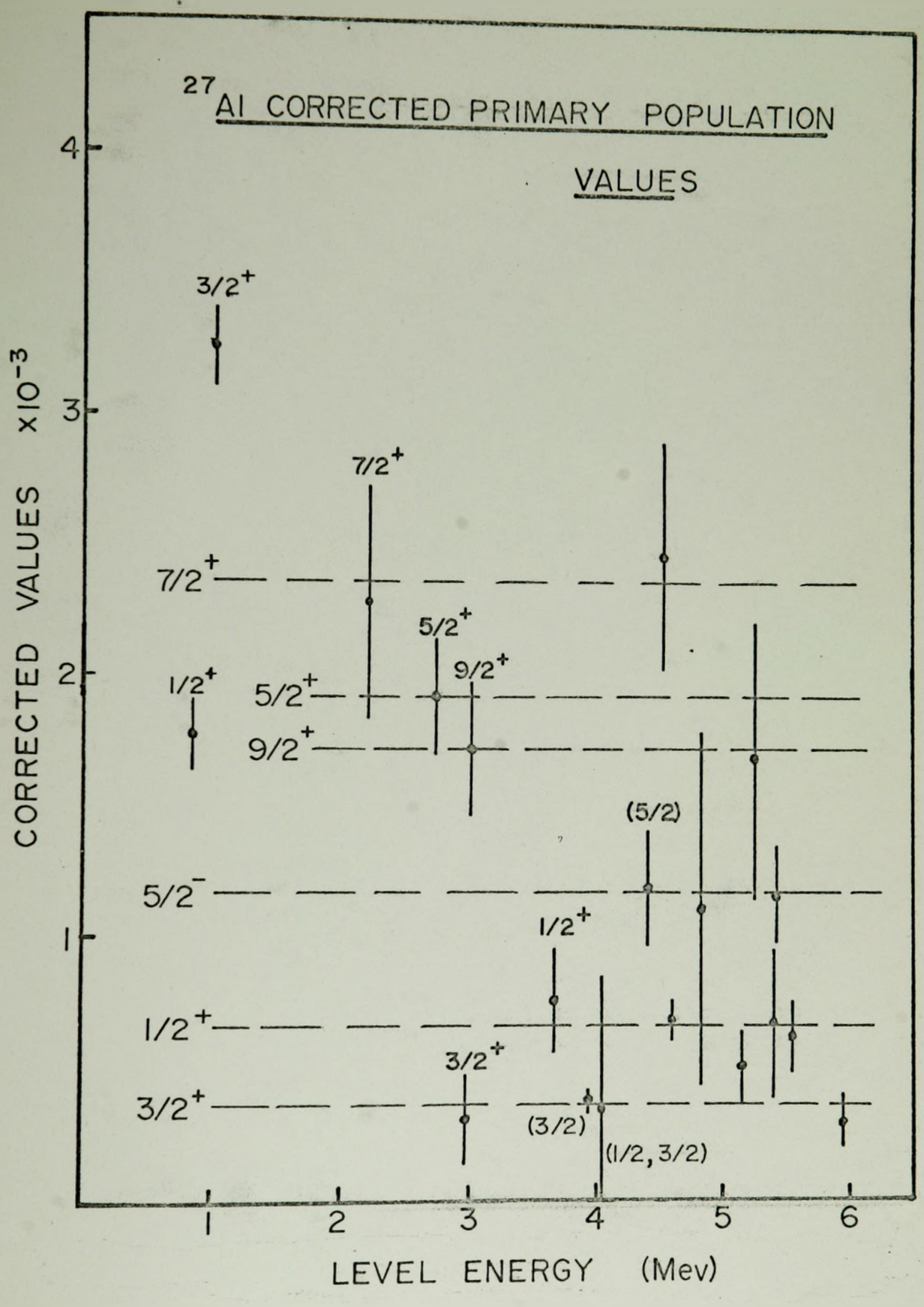
^{27}Al CORRECTED PRIMARY POPULATION VALUES
CORRECTED VALUES x10^{-3}
LEVEL ENERGY (Mev)
3/2$^+$
7/2$^+$
5/2$^+$
9/2$^+$
1/2$^+$
5/2$^-$
(5/2)
(3/2)
(1/2,3/2)

FIGURE 3-5

of decays to the ground state of ^{27}Mg were given by

$$I_G = I_{984} + \frac{30}{70} I_{952} + \frac{100}{70} I_{952} \qquad (3.1)$$

where I_G, I_{984} and I_{952} represent the relative intensities of the total number of transitions to the ground state, the relative intensity of the 984 keV γ-ray and the relative intensity of the 952 keV γ-ray. The contribution to the 1014 keV and 843.5 keV level were then calculated according to the β-decay branching ratio given in (8).

The above calculated primary population values as presented in Table III-6 were then plotted against the energy of the level concerned as shown in Fig. 3-4. The known spins (from (8)) were also noted and an attempt was made to fit a series of curves to these data similar to the curves for even-even nucleii as theorized by Feshbach (1). While curves could be fitted they led one more towards confusion than clarity.

The method of Donahue (2), however, as embodied in the flux and crossection correct values of Table III-6 and Figure 3-5 lead one to hazard the estimated spin assignments shown in the table.

3.3 Silicon

(a) γ-ray Energies

From Figure 2-1 one can see that the γ-ray spectrum arising from the inelastic scattering of neutrons from elemental silicon will contain γ-rays from three stable isotopes, ^{28}Si, ^{29}Si, and ^{30}Si in

addition to the background peaks already mentioned.

The same general procedures as described for the aluminum spectrum yielded the γ-ray energies, relative intensities, and assignments as presented in Table III-7. The aluminum (n, n', γ) lines arising out of scattering from the structural aluminum in the experimental facility now join the list of background lines seen in the spectra of the other elements examined. The 843.5 keV and 1014 keV γ-rays are the prominent ones seen. In addition one notices two other background peaks of unknown origin which were obscured in the aluminum spectrum. These are a γ-ray peak at 805 keV and a double escape peak at 3196 keV (4218").

Investigation of the competing neutron reactions

^{28}Si (n, γ) ^{29}Mg

^{28}Si (n, p) ^{28}Al

^{28}Si (n, d) ^{27}Al

yielded no conclusive evidence of their origin.

Some notable particulars of the listing in Table III-7 are lines number 2, 3, and 21. Line 2 (759 keV assumed) was left after subtracting the requirements for the double escape peak from line 8 out of the peak at 757 keV. Line 3 was split according to the requirements from (8) for the branching ratios of the 3507 keV and 1272 keV γ-rays from level B of ^{30}Si (see Figure 3-7). The decay of level J of ^{28}Si (see Figure 3-6) called for a 6019 keV γ-ray whose double escape peak could be hidden in the ^{57}Fe background double escape γ - ray peak at 4996 keV. By checking the relative peak heights of the two ^{57}Fe peaks at 4898 and 4996 keV in all the various (n, n', γ) spectra one could justify assigning the intensity

shown in Table III-7 for this line (line 21).

(b) Decay Schemes

The decay schemes worked out for the three isotopes are shown in Figures 3-6 and 3-7. In Table III-8 the energy levels measured and the branching ratios seen for ^{28}Si are compared with those of Endt et al (8) and (7). The 6019 keV and 1526 keV γ-rays called for in the decay of the 7798 keV level (8) were to have branching ratios of 75% and 25% respectively. As previously described one was able to justify a relative intensity of only 7(3) for the 6019 keV line which meant that the 1526 keV line, as reported, was probably too intense. By rechecking the other spectra one was able to find weak 1526 keV peaks in the background. As a result the reported branching ratio is actually based on the intensity of the 6019 keV line and (8).

The 1534 keV line can be shown to serve a dual role, either de-exciting the 8414 keV level of ^{28}Si or the 3767 keV level of ^{30}Si. Because of the lack of other helpful information the intensities of this γ-ray in each decay scheme is unknown. As mentioned above the decay of the 3507 keV level of ^{30}Si was calculated on the basis of the 3507 keV γ-ray intensity and the branching ratios from (8). The remaining intensity for the 1273 keV peak was assigned to the first state of ^{29}Si.

A case similar to this was made for the 2033 level of ^{29}Si where the 759 keV intensity reported was far to strong to be reasonable. In this case the transition was shown but the intensity is unknown.

TABLE III-7

γ-RAYS FROM Si(n, n', γ) Si SPECTRUM
(Excluding Background)

Line No.	γ-Ray Energy (keV)	Relative Intensity	Assignment
1	556 (4)	25 (7)	^{29}Si(E-D)+Background
2	(759)	(402)	^{29}Si(B-A)+Background
3	1273 (4) (1272)	178 (20) 15 (5)	^{29}Si(A-GND) ^{30}Si(B-A)
4	1526 (2)	38.5(16)	^{28}Si(J-D)+Background
5	1534 (3)	59 (23)	^{28}Si(N-F), ^{30}Si(C-A)
6	1591 (2)	73 (17)	^{29}Si(E-B)+Background
7	1664 (4)	45 (12)	^{28}Si(D-B)
8	1779 (4)	4250 (50)	^{28}Si(A-GND)
9	2033 (3)	70 (16)	^{29}Si(B-GND)
10	2235 (3)	80 (16)	^{30}Si(A-GND)
11	2433 (3)	32 (21)	^{29}Si(C-GND)
12	2835 (6)	144 (10)	^{28}Si(B-A)
13	3196 (6)	60 (6)	^{28}Si(C-A)
14	3507 (3)	12 (5)	^{30}Si(B-GND)
15	3931 (3)	16 (4)	^{28}Si(O-B)
16	4497 (3)	37 (4)	^{28}Si(D-A)
17	4911 (3)	9 (3)	^{28}Si(E-A)
18	5099 (3)	10 (4)	^{28}Si(F-A)
19	5108 (6)	6 (3)	^{28}Si(G-A)
20	5605 (8)	8 (3)	^{28}Si(H-A)
21	(6019)	7 (3)	^{28}Si(J-A)
22	6880 (3)	15 (3)	^{28}Si(F-GND)
23	6886 (3)	24 (3)	^{28}Si(G-GND)
24	7382 (2)	11 (3)	^{28}Si(H-GND)
25	7415 (4)	6 (3)	^{28}Si(I-GND)
26	7936 (6)	6 (3)	^{28}Si(K-GND)

TABLE III-8

^{28}Si BRANCHING RATIOS

Level	Present Work			Endt et al[8]		Endt et al[7]
	Level Energy*	Decay γ-rays	Branching Ratio+	Energy	Branching Ratio	Branching Ratio
A	1779 (4)	1779 (4)	100	1778.7(.2)	100	100
B	4614 (6)	2835 (6)	100	4614 (6) A	100	100
C	4975 (6)	3196 (6)	100	4975 (6) A	100	100
D	6277 (4)	4497 (3) 1664 (4)	45 (5) 55 (15)	6272 (6) A B	90 10	90 10
E	6690 (4)	4911 (3)	100	6690 (10) A	100	
F	6880 (3)	6880 (3) 5099 (3)	60 (12) 40 (16)	6878 (3) GND A	70 30	
G	6886 (3)	6886 (3) 5108 (6)	80 (10) 20 (10)	6887 (4) GND A	<1 100	
H	7383 (3)	7382 (2) 5605 (8)	57 (31) 43 (30)	7382 (8) GND A	45 55	45 55
I	7415 (4)	7415 (4)	100	7415 (8) GND A	90 10	90 10
J	7798 (3)	(6019) 1526 (2)	70 (30) 30 (20)	7798 (8) A D	75 25	
K	7936 (6)	7936 (6)	100	7932 (8) GND A	80 20	80 20

TABLE III-8 (cont'd.)

^{28}Si BRANCHING RATIOS

Level	Present Work			Endt et al[8]		Endt et al[7]
	Level Energy*	Decay γ-rays	Branching Ratio+	Energy	Branching Ratio	Branching Ratio
L				8260 (8)		
				GND	20	
				A	80	
M				8328		
				GND	55	55
				A	45	45
N	8414 (6)			8411 (8)		
		(1534)	100	F	86	
				A	8	
				B	4	
				D	2	
O	8545 (6)			8543 (8)		
		3931 (3)	100	B	100	

* All energies and errors, ( ), in keV

\+ Branching ratios and errors. ( ), in %

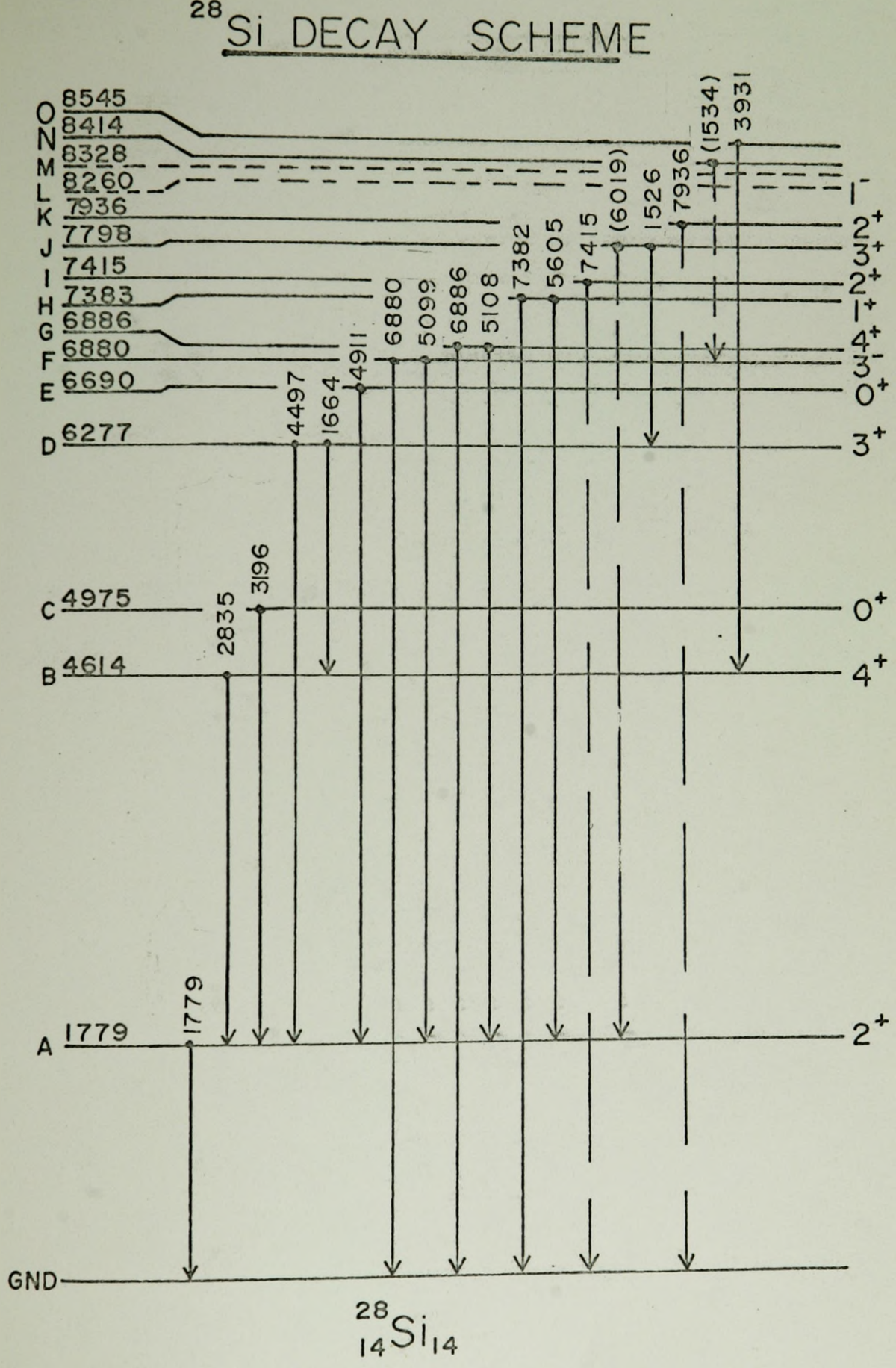
^{28}Si DECAY SCHEME
O 8545
N 8414
M 8328
L 8260
K 7936
J 7798
I 7415
H 7383
G 6886
F 6880
E 6690
D 6277
C 4975
B 4614
A 1779
GND
4497
1664
4911
6880
5099
6886
5108
7382
5605
7415
(6019)
1526
7936
(1534)
3931
3196
2835
1779
1⁻
2⁺
3⁺
2⁺
1⁺
4⁺
3⁻
0⁺
3⁺
0⁺
4⁺
2⁺
$^{28}_{14}$Si$_{14}$

FIGURE 3-6

^{29}Si AND ^{30}Si DECAY SCHEMES

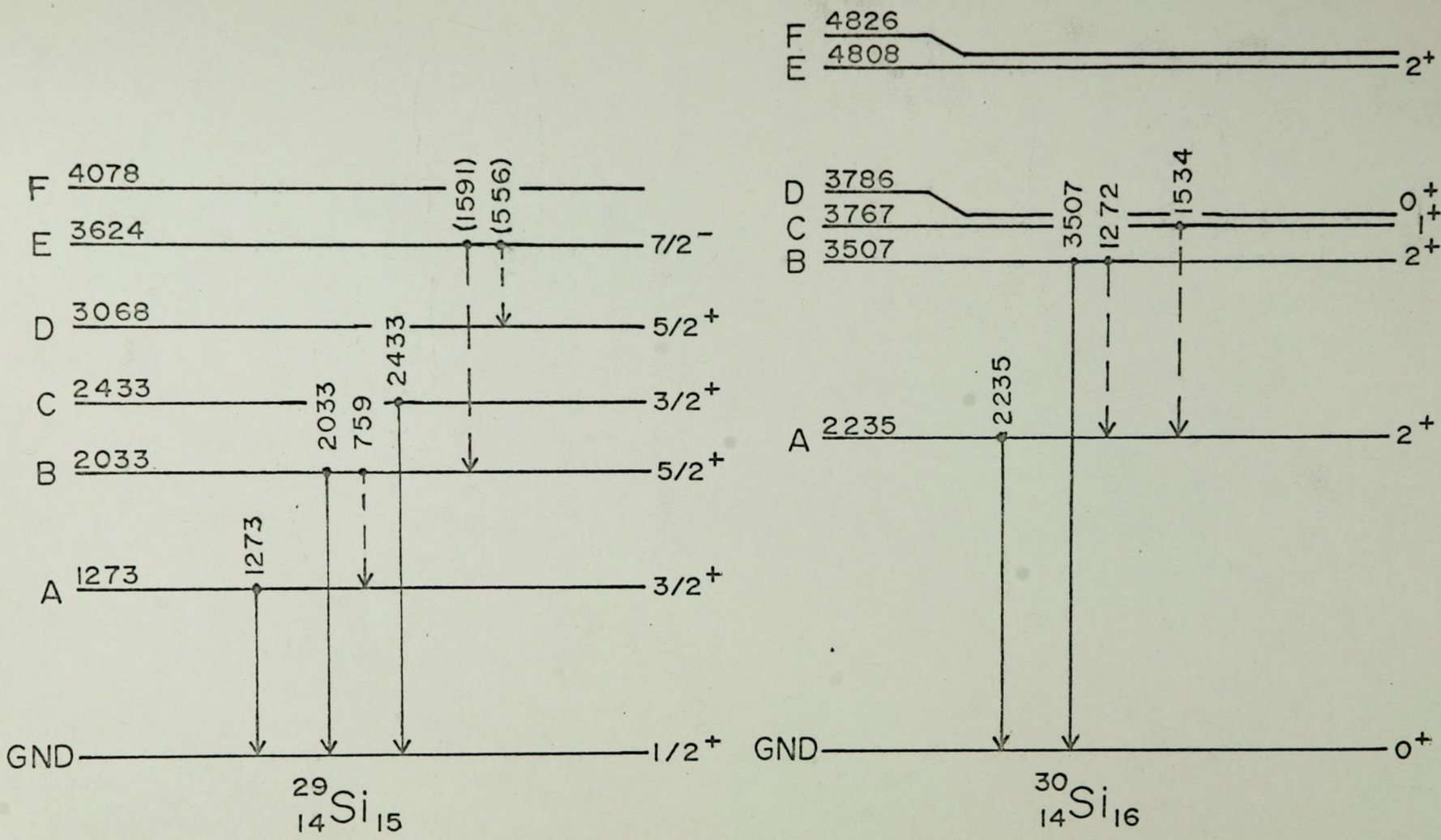

FIGURE 3-7

Likewise the two γ-rays from the 3624 level of ^{29}Si are shown but, again, their intensities are not known because of immersion in background peaks. The background also renders the intensity of the 1664 keV γ-ray from level D of ^{28}Si suspect as further implied by the lack of agreement with either (8) or (7) for the branching ratios of the 6277 keV level.

The only major disagreement with previous branching ratios for ^{28}Si occurs in the decay of the 6886 keV level.

The decay schemes for ^{29}Si and ^{30}Si as presented in Figure 3-7 have already been discussed. They agree with (8) for all transitions shown and those not seen but reported in (8) can be discounted on the basis of low intensity and low isotopic abundance.

Previously reported (n, n', γ) work in (10) indicates that the only γ-rays seen were the 1.78 Mev γ-ray in ^{28}Si, the 1.28 Mev γ-ray in ^{29}Si, and the 1.28 and 2.2 Mev γ-rays in ^{30}Si.

(c) Primary Population of Levels

Because of poor statistics and uncertain intensities in ^{29}Si and ^{30}Si only the levels in ^{28}Si were submitted to investigation for relative primary population values. These are presented, as calculated by the methods of Section 2.5 (e) in Table III-9.

The relative primary population values are plotted in Figure 3-8 do not fit the calculated curves for A=28 shown in Fig. 1-3 with any great degree of uncertainty. Even keeping the same slope, but adjusting the curves laterally with respect to one another as shown, fails to give a good fit. Attempts to improve the fit result in a faster falloff of values with energy than that predicted from (1).

TABLE III-9

PRIMARY POPULATION VALUES FOR ^{28}Si

Level	Energy	Spin (from (8))	Relative Primary Population Value	Corrected Relative Population Value
GND		0^+		
A	1779	2^+	3969 (86)	11495 (249)
B	4614	4^+	83 (25)	1317 (398)
C	4975	0^+	60 (6)	1176 (118)
D	6277	3^+	79 (18)	3432 (783)
E	6690	0^+	9 (3)	500 (165)
F	6880	3^-	<25 (7)	<1562 (44)
G	6886	4^+	30 (6)	1875 (375)
H	7383	1^+	19 (6)	1800 (500)
I	7415	2^+	7 (3)	608 (260)
J	7798	3^+	10 (5)	1088 (544)
K	7936	2^+	7 (3)	824 (350)
L	8260	1^-		
M	8328			
N	8414		59 (23)$^+$	
O	8545	[4]	16 (4)	2712 (678)

[ ] Spin predicted from Fig. 3-8.

$^+$ too high a value to be reasonable.

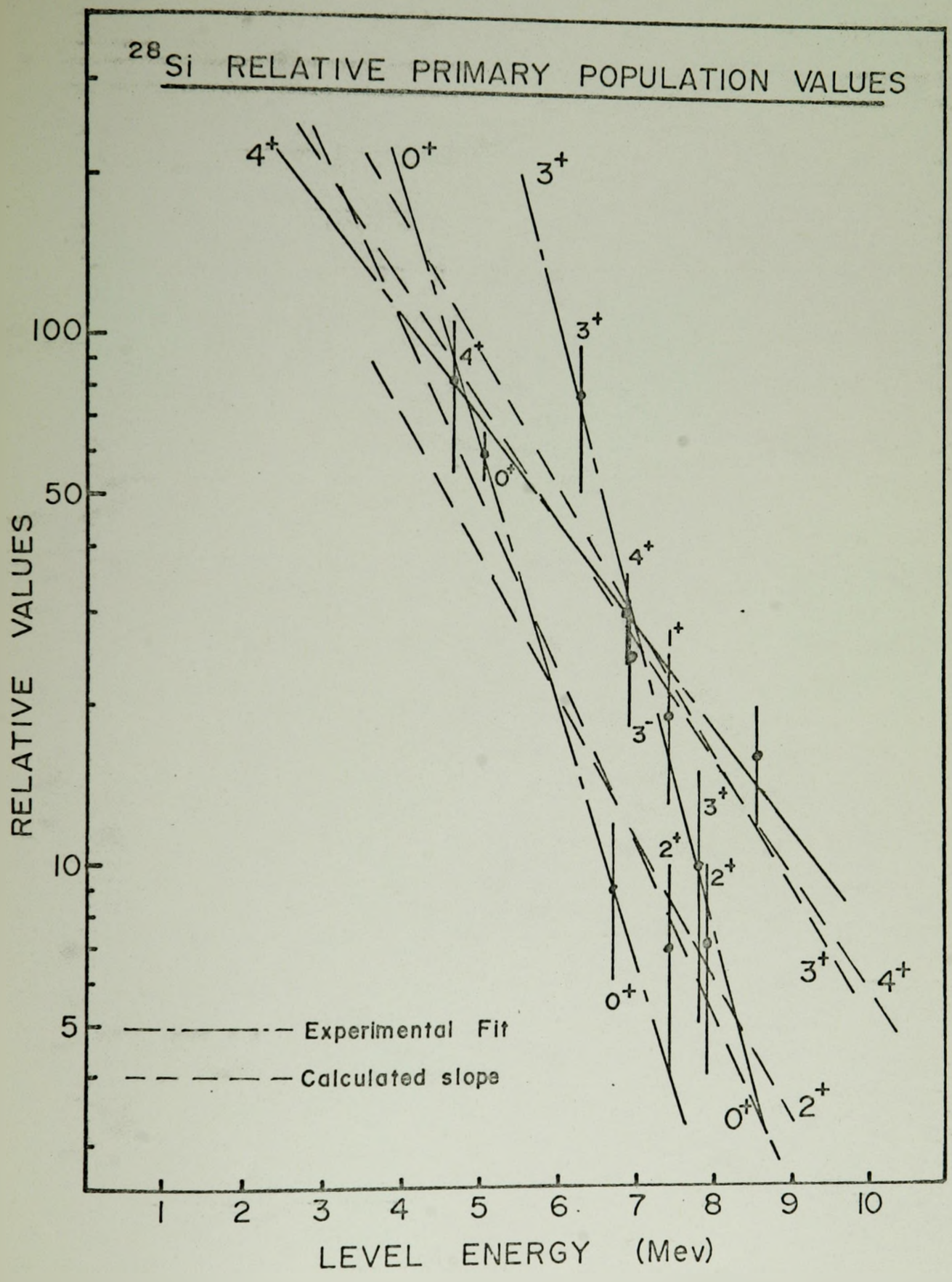
^{28}Si RELATIVE PRIMARY POPULATION VALUES
RELATIVE VALUES
100
50
10
5
1
2
3
4
5
6
7
8
9
10
LEVEL ENERGY (Mev)
Experimental Fit
Calculated slope
4+
0+
3+
4+
3+
0+
4+
1+
3-
3+
2+
2+
0+
3+
4+
0+
2+

FIGURE 3-8

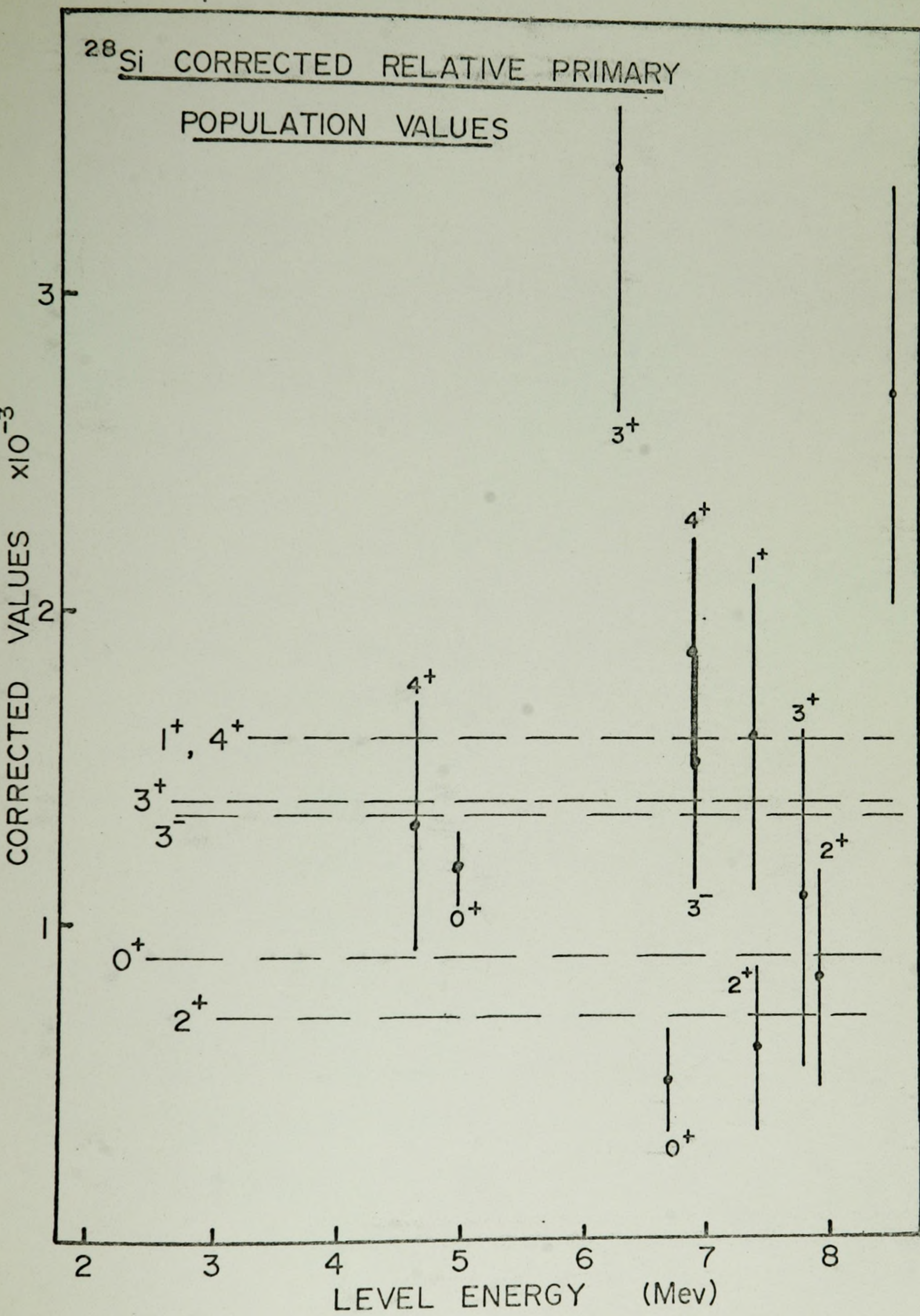

28Si CORRECTED RELATIVE PRIMARY
POPULATION VALUES
CORRECTED VALUES x10^-3
LEVEL ENERGY (Mev)
1
2
3
2
3
4
5
6
7
8
1+, 4+
3+
3-
0+
2+
4+
0+
3+
4+
1+
3+
3-
2+
0+
2+

FIGURE 3-9

Because of the invalidity below ~2 Mev of the neutron flux distribution used to generate these curves points below 2Mev were treated cautiously in all analysis of this type. However, on the basis of this plot, one hazards an estimate of a J value of 4 for the 8545 keV level.

The corrected values, using the method of Donahue (2), plotted in Fig. 3-9 do not fare any better and tend to make the J=4 estimates above rather doubtful.

3.4 Phosphorus

(a) γ-ray Energies

Like aluminum, natural phosphorus presents one with a monoisotopic target to analyse. The γ-rays from the analysis of the ^{31}P spectrum along with their relative intensities and assignments, as deduced by the methods previously discussed, appear in Table III-10.

Investigation of the competing neutron reactions yield evidence of the following reactions.

$$^{31}P\ (n,\ \alpha,\ \gamma)\ ^{28}Al\ (\beta,\ \gamma)\ ^{28}Si$$

$$^{31}P\ (n,\ p,\ \gamma)\ ^{31}Si$$

The 1272 keV and 2240 keV γ-rays, suggested by (8), were assumed to be hidden in the adjacent peaks. Their relative intensities were then calculated from the intensity of the 3506 keV γ-ray using the branching ratios of (8). Likewise, the intensity of the 1016 keV γ-ray from the 4431 keV level, hidden in the 1014 keV background peak of $^{27}Al\ (n,\ n',\ \gamma)$, was calculated in the same manner.

(b) Decay Scheme

The decay scheme presented in Fig. 3-10 and as summarized in Table III-11 agrees very well with previous data from (8) in all

TABLE III-10

γ-RAYS FROM $^{31}P(n, n, \gamma)\ ^{31}P$ SPECTRUM

Line No.	γ-ray Energy*	Relative Intensity	Assignment
1	752 (3)	52 (7)	$^{31}P(n,p,\gamma)^{31}Si$
2	968 (2)	28 (9)	2234-1266+Background
3	983 (3)	15 (9)	$^{31}P(n,\alpha,\gamma)^{28}Al$
4	1016 (8)	44 (20)	4431-3414, $^{31}P(n,\alpha,\gamma)^{28}Al$
5	1137 (3)	50 (9)	4431-3295
6	1266 (3)	1400 (15)	1266-0
7	(1272)		3506-2234
8	1695 (5)	49 (12)	$^{31}P(n,p,\gamma)^{31}Si$
9	1781 (4)	85 (12)	$^{31}P(n,\alpha)^{28}Al(\beta,\gamma)^{28}Si$
10	2025 (2)	39 (25)	4260-2234
11	2029 (2)	98 (15)	3295-1266
12	2149 (4)	97 (13)	3415-1266
13	2199 (4)	60 (5)	4431-2234
14	2234 (4)	345 (16)	2234-0
	(2240)	15 (2)	3506-1266
15	2926 (2)	48 (8)	4190-1266
16	2994 (3)	32 (12)	4260-1266
17	3135 (3)	38 (5)	3135-0
18	3328 (3)	13 (4)	4592-1266
19	3506 (8)	27 (4)	3506-0
20	3654 (4)	10.5 (4)	5892-2234
21	3748 (2)	9 (3)	5015-1266
22	4263 (6)	16 (3)	4260-0
23	4591 (5)	5 (3)	4592-0
24	5019 (8)	14.5 (3)	5015-0
25	5559 (5)	6 (2)	5557-0

* All energies and their errors, ( ), are in keV.

TABLE III-11

^{31}P BRANCHING RATIOS

Level	Present Work			Endt et al[8]		Endt et al[7]
	Level Energy*	Decay γ-rays	Branching Ratio+	Energy	Branching Ratio	Branching Ratio
A	1266 (3)	1266 (3)	100	1266.1(.2)	100	100
B	2234 (4)	2234 (4)	93 (4)	2233.8(.5)		
		968 (2)	7 (3)	GND	100	> 97
				A	< 1	
C	3135 (3)	3135 (3)	100	3134.7(.5)		
				GND	100	> 80
				B	< 1	
				A	< 1	
D	3295 (4)	2029 (2)	100	3294.9(.4)		
				A	80	45 (> 87)
				B	20	45
				GND		10
E	3415 (3)	2149 (2)	100	3414.2(.6)		
				A	100	85
				GND	< 1	15
				B	< 2	
F	3506 (8)	3506 (8)	60	3505.5(1.0)		
		(2240)	35 +	GND	60	>90
		(1272)	5 +	A	> 35	
				B	< 5	
G	4192 (4)	2926 (2)	100	4190.3(1.0)		
				A	75	65
				B	25	35
H	4260 (3)	4263 (6)	27 (5)	4260.4(1.5)		
		2994 (3)	53 (20)	GND	75	
		2025 (2)	20 (3)	A	20	60
				B	5	40
I	4432 (4)	2199 (4)	50 (12)	4431.0(9)		
		1137 (3)	45 (15)	B	55	60
		(1016)	(5)	D	40	15
				E	5	
				GND		25

TABLE III-11 (cont'd.)

^{31}P BRANCHING RATIOS

Level	Present Work			Endt et al[8]		Endt et al[7]
	Level Energy*	Decay γ-rays	Branching Ratio+	Energy	Branching Ratio	Branching Ratio
J	4592.5 (3)			4592.4		
		4591 (5)	23 (13)	GND	25	
		3328 (3)	59 (18)	A	55	
		(2358)	20	B	20	
				D		100
M	5015 (4)			5015.4		
		5015 (8)	61 (10)	GND	70	>70
		3748 (4)	39 (12)	A	30	
R	5559 (2)			5557 (2)		
		5559 (2)	100	GND	100	
U	5888 (4)			5892 (2)		
		3654 (2)	100	B	100	

* All energies and errors, ( ), in keV.

\+ Branching ratios and errors, ( ), in %

^{31}P DECAY SCHEME

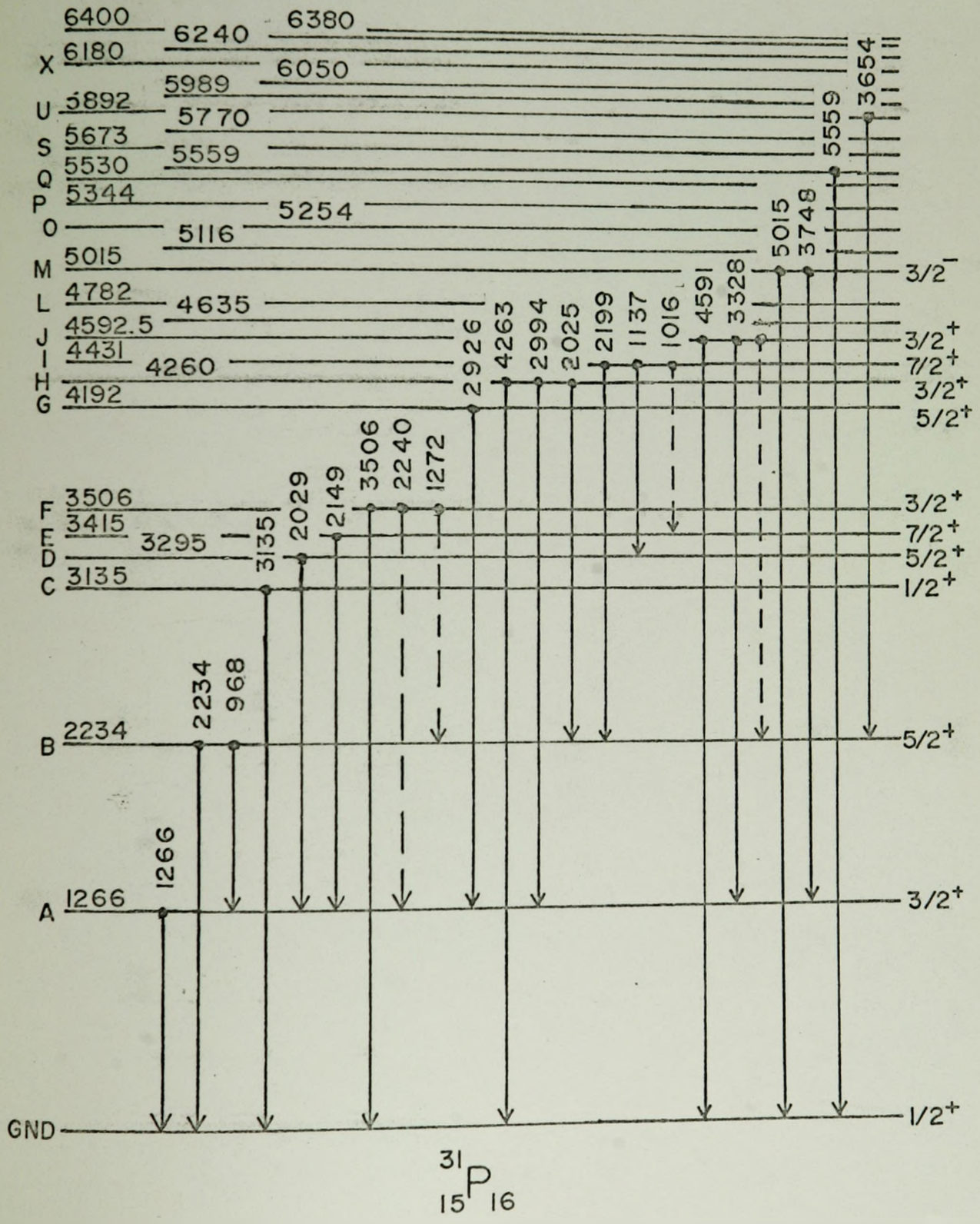

FIGURE 3-10

TABLE III-12

PRIMARY POPULATION VALUES FOR ^{31}P

Level	Level Energy	Spin (from (8))	Relative Primary Population Value	Corrected Values
GND	0	$1/2^+$		
A	1266	$3/2^+$	1060 (80)	2230 (170)
B	2234	$5/2^+$	291 (37)	1100 (140)
C	3135	$1/2^+$	37 (15)	239 (165)
D	3295	$5/2^+$	73 (27)	521 (193)
E	3415	$7/2^+$	91 (15)	700 (115)
F	3506	$3/2^+$	43 (7)	344 (56)
G	4192	$5/2^+$	* 63 (11)	776 (135)
H	4260	$3/2^+$	* 60 (17)	760 (216)
I	4431	$7/2^-$	* 116 (16)	1656 (228)
J	4592.5	$3/2^+$	22 (9)	344 (140)
M	5015	$3/2^-$	24 (6)	480 (120)
R	5559	(3/2) $1/2^+$	6 (2)	165 (55)
U	5888	$3/2^+$	10.5(4)	362 (140)

Spins predicted from Fig. 3-12

* These levels include calculated intensities from γ-rays suggested by (8) but too weak to be observed in the present work.

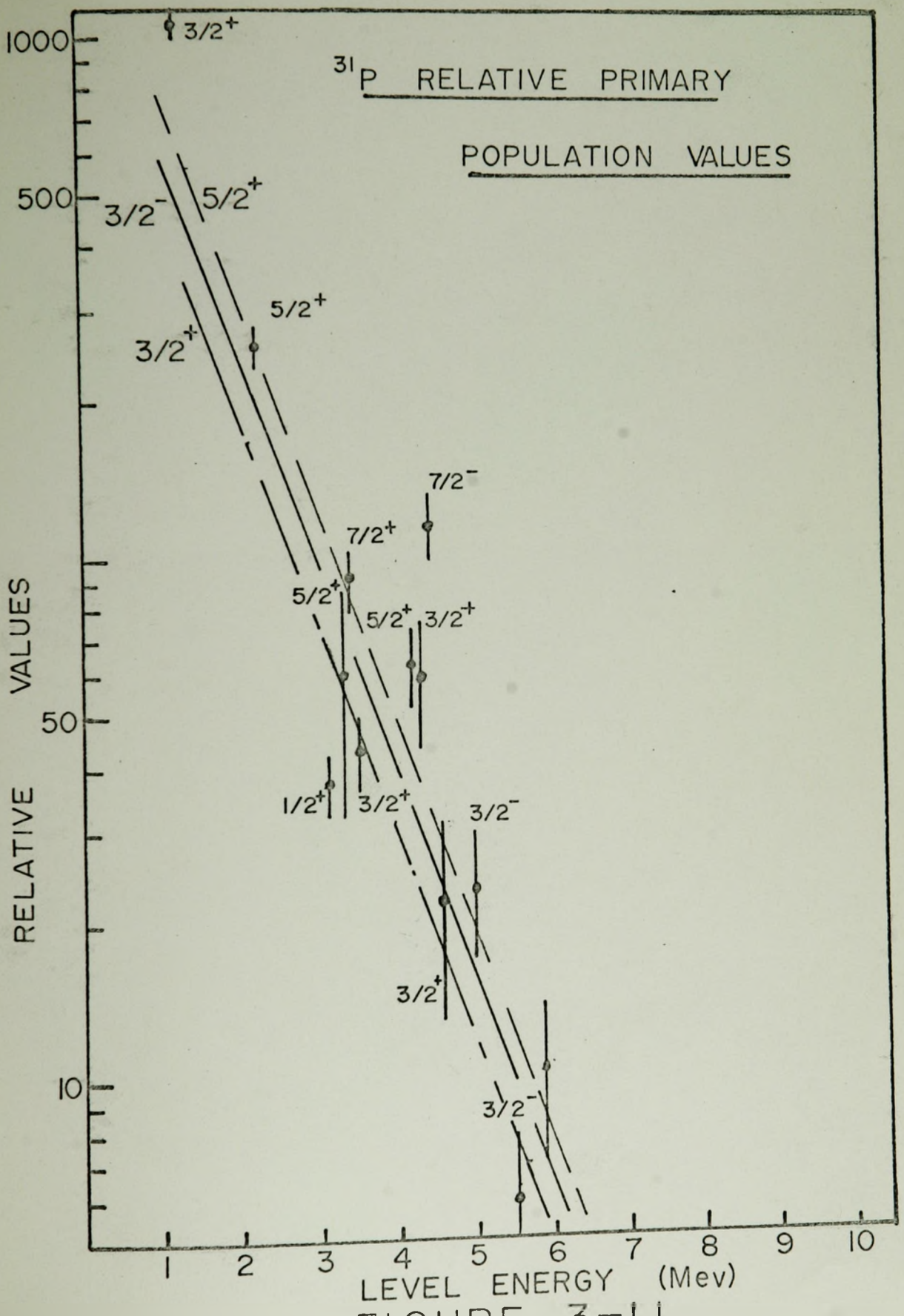
^{31}P RELATIVE PRIMARY
POPULATION VALUES
RELATIVE VALUES
1000
500
50
10
3/2+
3/2-
5/2+
5/2+
3/2+
7/2-
7/2+
5/2+
5/2+
3/2+
1/2+
3/2+
3/2-
3/2+
3/2-
1
2
3
4
5
6
7
8
9
10
LEVEL ENERGY (Mev)

FIGURE 3-11

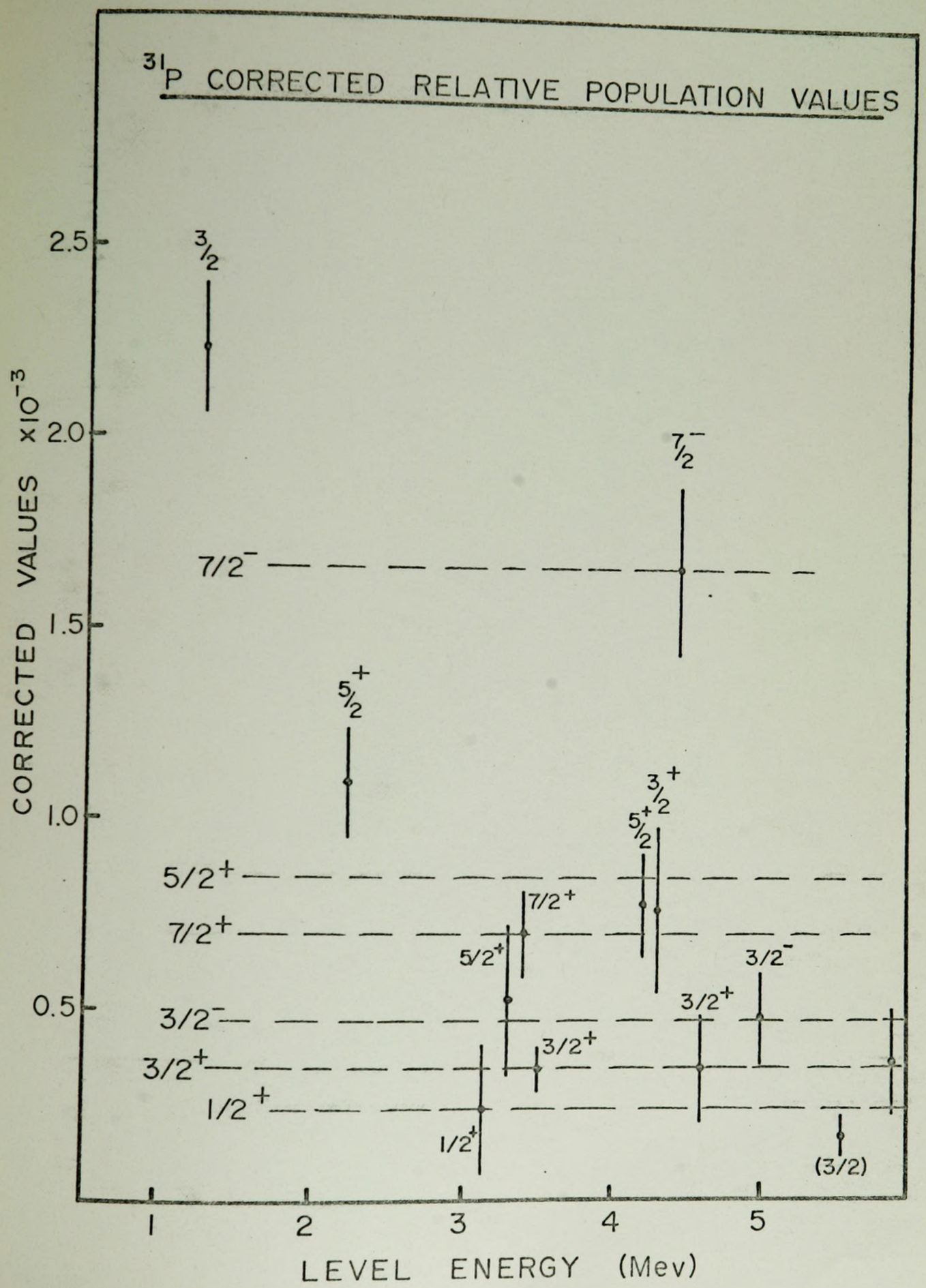
^{31}P CORRECTED RELATIVE POPULATION VALUES
CORRECTED VALUES x10^{-3}
2.5
2.0
1.5
1.0
0.5
3/2
7/2$^-$
7/2$^-$
5/2$^+$
5/2$^+$
3/2$^+$
7/2$^+$
5/2$^+$
7/2$^+$
5/2$^+$
3/2$^-$
3/2$^-$
3/2$^+$
3/2$^+$
3/2$^+$
1/2$^+$
1/2$^+$
(3/2)
1
2
3
4
5
LEVEL ENERGY (Mev)

FIGURE 3-12

but one case: the decay of the 4260 keV level. Some multiple de-excitation branches called for by (8) were not observed due to the low relative intensities involved. Several levels, however, do support (8) against the data of (7).

The previously reported γ-rays seen from inelastic neutron scattering as summarized in (10) include only the three γ-rays involved in the de-excitation of the first two levels of ^{31}P and agree with the present work, within their errors.

(c) Primary Population of Levels

As in the previous cases the calculated relative primary population values, as tabulated in Table III-12, were plotted as shown in Fig. 3-11. The spin assignments given in (8) allow one to attempt to fit curves to the $3/2^+$ and $5/2^+$ states as shown. One cannot compare these curves to the theory of Feshback (1), however, because one is dealing with an odd-even nucleus.

The method of Donahue (2) yields the corrected values listed in Table III-12 and plotted in Figure 3-12. On the basis of this plot one can hazard an estimate of spin $3/2^+$ for the 5088 keV level and a spin of $1/2^+$ for the 5559 keV level, placing its previous estimate (8) of (3/2) in doubt.

3.5 Sulphur

(a) γ-ray Energies

Although there are four stable isotopes in elemental sulphur two of these, because of their very low natural abundance, play insignificant roles in the analysis of the present inelastic scattering work. The other two, however, can be readily seen as an examination of Table III-13

will reveal.

From Figure 2-1 one sees that ^{32}S is about 19 times as abundant as ^{34}S, justifying the observation of many more γ-rays from ^{32}S than from ^{34}S. The γ-rays and their respective properties, as presented for previously discussed elements, are given in Table III-13.

In this case there is evidence of two competing neutron reactions, namely, the familiar ^{32}S (n,p) ^{32}P reaction and the ^{32}S (n, α) ^{29}Si reaction. Line 4 can be suggested to arise from ^{33}S but its intensity is undeterminable because of the ^{27}Al background peak masking it.

(b) Decay Schemes

The decay schemes for ^{32}S and ^{34}S as suggested by Endt et al (8) and supported by the present work are shown in Figure 3-13. Once again one has a called for γ-ray hidden in another major peak, namely, the de-excitation γ-ray from the 4465 keV level to the 2230 keV level.

The comparisons of present results with that of Endt et al (7) and (8) are presented in Table III-14 and tend to be in agreement except for a few points. One of these is the branching ratios from level E which seems to be at odds with the values of Endt et al. Levels C and L are in obvious disagreement with (7) and (8) while levels H and J tend to support the values of (7) over (8).

In the ^{34}S decay scheme a 3300 keV γ-ray is called for in partnership with the 1173 keV γ-ray from level B but is not observed.

Previous reports in the literature (10) for (n, n', γ) work,

TABLE III-13

γ-RAYS FROM S(n, n', γ) S SPECTRUM

Line No.	γ-Ray Energy*	Relative Intensity	Assignment
1	612 (3)	17 (6)	^{34}S (C-B)
2	638 (3)	14 (6)	^{32}S(n,p,γ)^{32}P
3	771 (2)	9 (6)	^{34}S (D-B)
4	(842)		^{33}S(A-GND)+Background
5	1071 (2)	22 (9)	^{32}S(n,p,γ)^{32}P
6	1149 (3)	18 (9)	^{32}S(n,p,γ)^{32}P
7	1173 (4)	38 (10)	^{34}S (B-A)
8	1243 (3)	45 (10)	^{32}S(n,p,γ)^{32}P
9	1274 (3)	114 (11)	^{32}S(n,α,γ)^{29}Si
10	1323 (3)	46 (11)	^{32}S(n,p,γ)^{32}P
11	1548 (4)	60 (9)	^{32}S (B-A)
12	1676 (4)	68 (16)	^{32}S(n,p,γ)^{32}P
13	2032 (4)	18 (13)	^{32}S(n,α,γ)^{29}Si
14	2054 (4)	31 (14)	^{32}S (C-A)
15	2127 (4)	43 (15)	^{34}S (A-GND)
16	2230 (6)	451 (20)	^{32}S (A-GND)
17	(2235)		^{32}S (D-A)
18	2462 (4)	78 (10)	^{32}S (E-A)
19	2780 (3)	47 (20)	^{32}S (F-A)
20	3177 (4)	13 (6)	^{32}S (G-A)
21	3327 (4)	19 (11)	^{32}S (H-A)
22	3998 (4)	10 (3)	^{32}S (J-A)
23	4212 (5)	11 (3)	^{32}S (K-A)
24	4283 (5)	33 (4)	^{32}S (C-GND)
25	4394 (3)	12 (3)	^{32}S (L-A)
26	4692 (4)	10 (4)	^{32}S (E-GND)
27	5555 (4)	6 (3)	^{32}S (H-GND)
28	6230 (4)	7 (3)	^{32}S (J-GND)

* All energies and errors, ( ), in keV.

TABLE III-14

^{32}S BRANCHING RATIOS

Level	Present Work			Endt et al[8]		Endt et al[7]
	Level Energy *	Decay γ-rays	Branching Ratio+	Energy	Branching Ratios	Branching Ratios
A	2230 (6)	2230 (6)	100	2237 (4) GND	100	100
B	3778 (6)	1548 (4)	100	3780 (8) A GND	100 <0.2	100 <0.2
C	4284 (4)	4283 (5) 2054 (4)	52 (6) 48 (20)	4287 (8) GND A	90 10	90 10
D	(4465)	(2235)	?	4465 (10) A	100	100
E	4692 (4)	2462 (4) 4692 (4)	89 (11) 11 (5)	4698 (10) A GND	65 35	70 30
F	5010 (4)	2780 (3)	100	5012 (8) A	100	100
G	5407 (6)	3177 (4)	100	5410 (20) A GND	96 4	
H	5556 (3)	3327 (4) 5555 (4)	76 (44) 24 (12)	5553 (8) A GND	55 45	60 40
J	6229 (4)	3998 (4) 6230 (4)	59 (18) 41 (18)	6226 (8) A GND	100	75 25
K	6442 (5)	4212 (5)	100	6440 (20) A	100	
L	6624 (4)	4394 (3)	100	6621 (8) A F	10 90	20 80

* All energies and errors, ( ), in keV

\+ Branching ratios and errors, ( ), in %

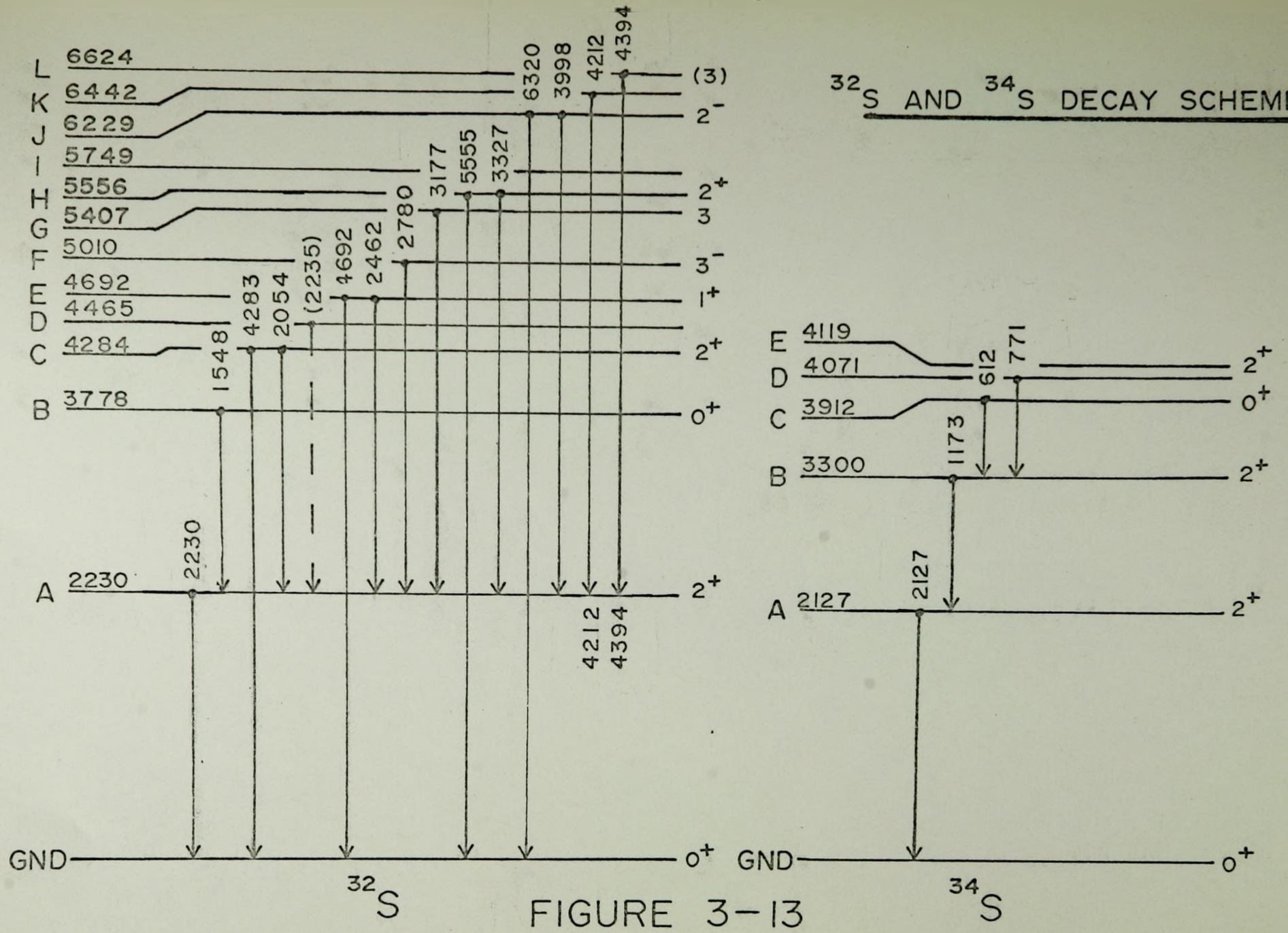
32S AND 34S DECAY SCHEMES
L
K
J
I
H
G
F
E
D
C
B
A
6624
6442
6229
5749
5556
5407
5010
4692
4465
4284
3778
2230
6320
3998
4212
4394
3177
5555
3327
2780
4692
2462
(2235)
2054
4283
1548
2230
(3)
2-
2+
3-
2+
0+
2+
GND
0+
32S
4119
4071
3912
3300
2127
612
771
1173
2127
2+
0+
2+
2+
GND
0+
34S

FIGURE 3-13

TABLE III-15

PRIMARY POPULATION VALUES FOR ^{32}S

Level	Energy	Spin (from (e))	Relative Primary Population Value	Corrected Values
GND		0^+		
A	2230	2^+	171 (100)	360 (210)
B	3778	0^+	60 (9)	572 (86)
C	4284	2^+	64 (18)	830 (235)
D	4465		?	
E	4692	1^+	88 (14)	1466 (233)
F	5010	3^-	47 (20)	960 (410)
G	5407	3	13 (6)	333 (154)
H	5556	2^+	25 (14)	695 (390)
J	6229	2^-	17 (6)	680 (150)
K	6442	[0, 2, 3]	11 (3)	525 (150)
L	6624	(3)	12 (3)	665 (167)

[ ] Spin predicted from Fig. 3-15.

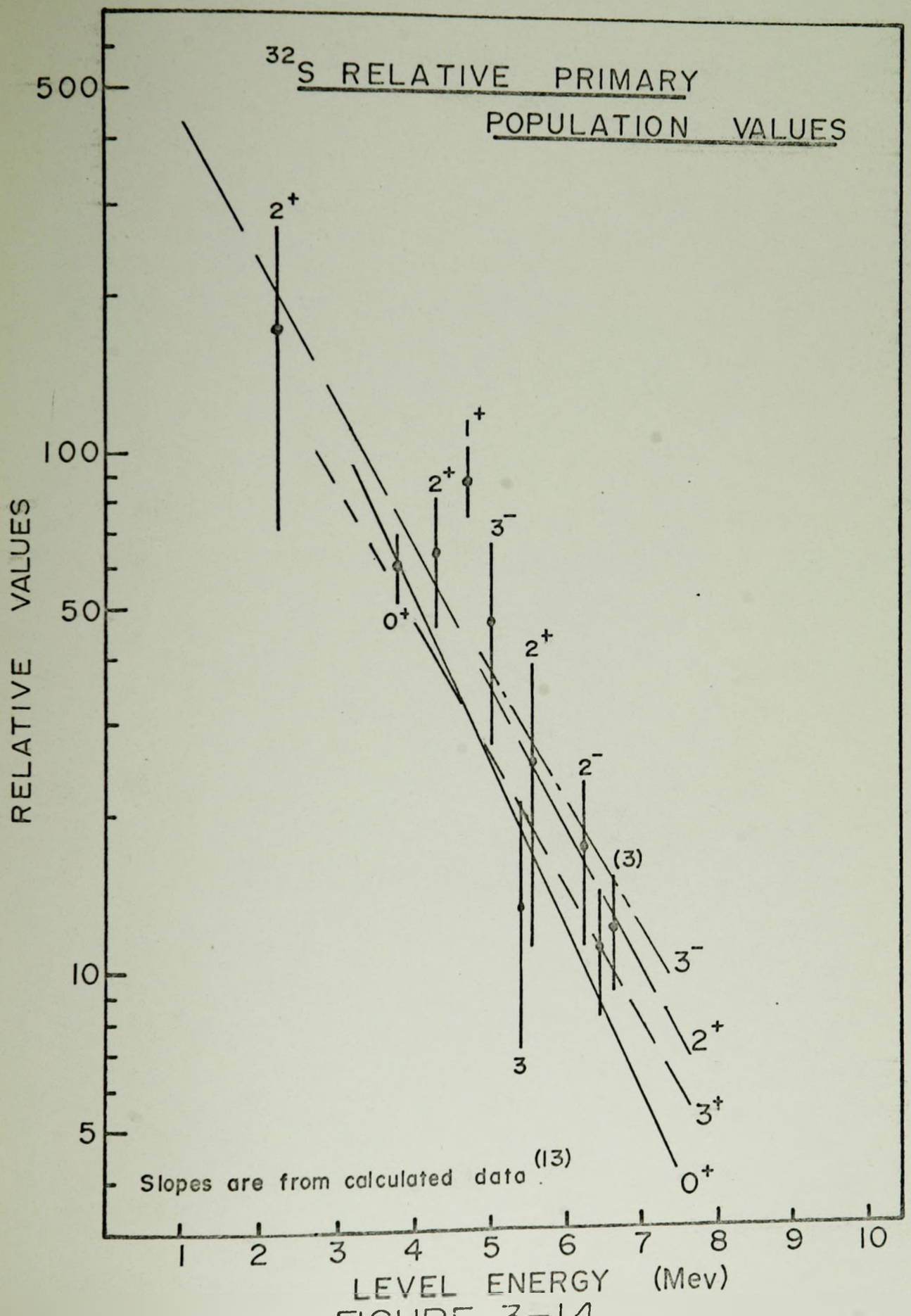
^{32}S RELATIVE PRIMARY
POPULATION VALUES
RELATIVE VALUES
500
100
50
10
5
2⁺
1⁺
2⁺
3⁻
0⁺
2⁺
2⁻
(3)
3
3⁻
2⁺
3⁺
0⁺
Slopes are from calculated data (13)
1
2
3
4
5
6
7
8
9
10
LEVEL ENERGY (Mev)

FIGURE 3-14

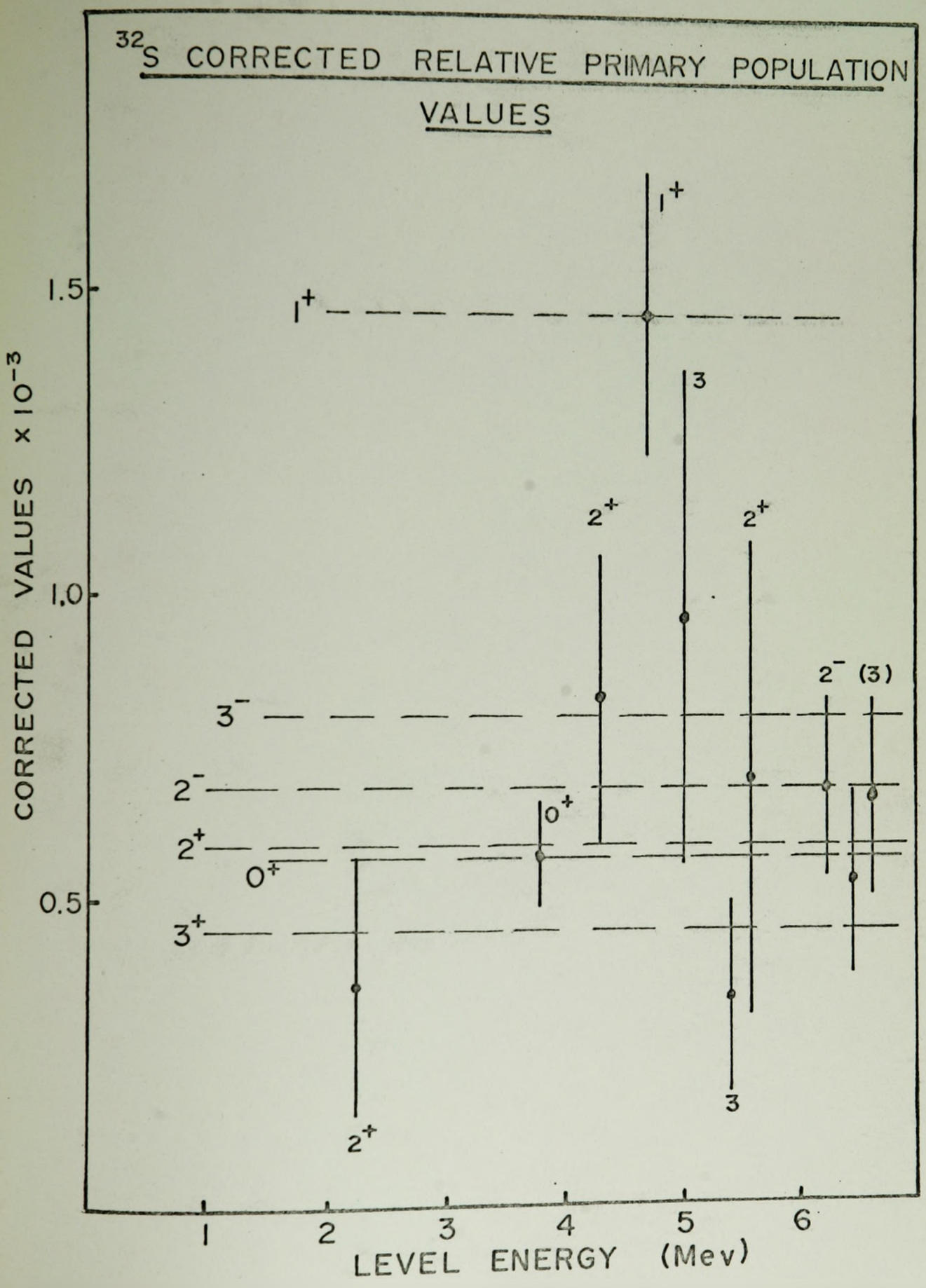
32S CORRECTED RELATIVE PRIMARY POPULATION VALUES
CORRECTED VALUES x 10-3
1.5
1.0
0.5
1+
3
2+
2+
2- (3)
3-
2-
0+
2+
0+
3+
2+
3
1
2
3
4
5
6
LEVEL ENERGY (Mev)

FIGURE 3--15

report seeing only the 2.23 Mev level of ^{32}S with values in the range from 2.20 to 2.32 Mev.

(c) Primary Population of Levels

Since ^{32}S is an even-even nucleus one can apply curves generated from (1) to the relative primary population values as tabulated in Table III-15 and shown in Fig. 3-14. In this case there is better agreement with the calculated curves than in the case of ^{28}Si but the 1^+ state seems to be out of place.

The corrected values are shown in Figure 3-15. From these one would predict a J value of 0, 2 or 3 for the 6442 keV level. This is supported by the data of Figure 3-14.

Due to incompleteness and poor statistics the ^{34}S decay scheme was not subjected to the above analysis.

3.6 Chlorine

(a) γ-ray Energies

In the inelastic neutron scattering γ-ray spectrum from elemental chlorine one is concerned with two isotopes, ^{35}Cl and ^{37}Cl (see Figure 2-1.) The analysis was straight forward, however, with the resulting γ-rays and their relative intensities and assignments presented in Table III-16. One competing neutron reaction was observed. This was the ^{35}Cl (n, α, γ) ^{32}P reaction as noted in the table.

(b) Decay Schemes

The decay schemes for ^{35}Cl and ^{37}Cl as worked out are given in Figure 3-16. For ^{35}Cl the energy levels and branching ratios are compared with previous values, as given by Endt et al (7) and (8),

TABLE III-16

γ-RAYS FROM Cl (n, n', γ) Cl SPECTRUM

Line No.	Energy* of γ-ray	Relative Intensity	Assignment
1	833 (4)	71 (11)	^{37}Cl (A-GND)
2	1071 (4)	32 (14)	^{35}Cl(n,α,γ)^{32}P+Background
3	1219 (4)	680 (19)	^{35}Cl (A-GND)
4	1240 (3)	55 (16)	^{35}Cl(n,α,γ)^{32}P+ ^{35}Cl(E-B)
5	1323 (4)	115 (18)	^{35}Cl(n,α,γ)^{32}P+Background
6	1427.5 (3)	52 (19)	^{35}Cl (C-A)
7	1480 (3)	55 (20)	^{35}Cl (D-A)
8	1726 (4)	188 (24)	^{37}Cl (B-GND)
9	1762.5 (4)	902 (24)	^{35}Cl (B-GND)
10	1786 (3)	38 (22)	^{35}Cl (E-A)
11	1891 (3)	82 (22)	^{37}Cl (E-B)
12	1940 (3)	86 (23)	^{35}Cl (F-A)
13	2249 (3)	93 (28)	^{37}Cl (C-A)
14	2647 (5)	214 (20)	^{35}Cl (C-GND)
15	2694.5 (4)	140 (10)	^{35}Cl (D-GND)
16	2839 (4)	45 (13)	^{35}Cl (G-A)
17	2895 (5)	22 (12)	^{35}Cl (H-A)
18	2952.5 (3)	28 (11)	^{35}Cl (I-A)
19	3004 (8)	126 (11)	^{35}Cl (E-GND)
20	3087 (5)	124 (31)	^{37}Cl (C-GND)
21	3105 (4)	120 (30)	^{37}Cl (D-GND)
22	3163 (4)	215 (20)	^{35}Cl (F-GND)
23	3620 (4)	30 (7)	^{37}Cl (E-GND)
24	3746 (4)	38 (7)	^{37}Cl (F-GND)
25	4056 (4)	13 (5)	^{35}Cl (G-GND)
26	4113 (4)	21 (5)	^{35}Cl (H-GND)
27	4174 (4)	32 (6)	^{35}Cl (I-GND)
28	4324 (4)	110 (49)	^{37}Cl (G-GND)
29	5031 (4)	15 (4)	^{35}Cl (J-GND)
30	5220 (6)	10 (4)	^{35}Cl (K-GND)
31	5416 (8)	25 (4)	^{37}Cl (H-GND)

* All energies and errors ( ) in keV.

^{35}Cl AND ^{37}Cl DECAY SCHEMES

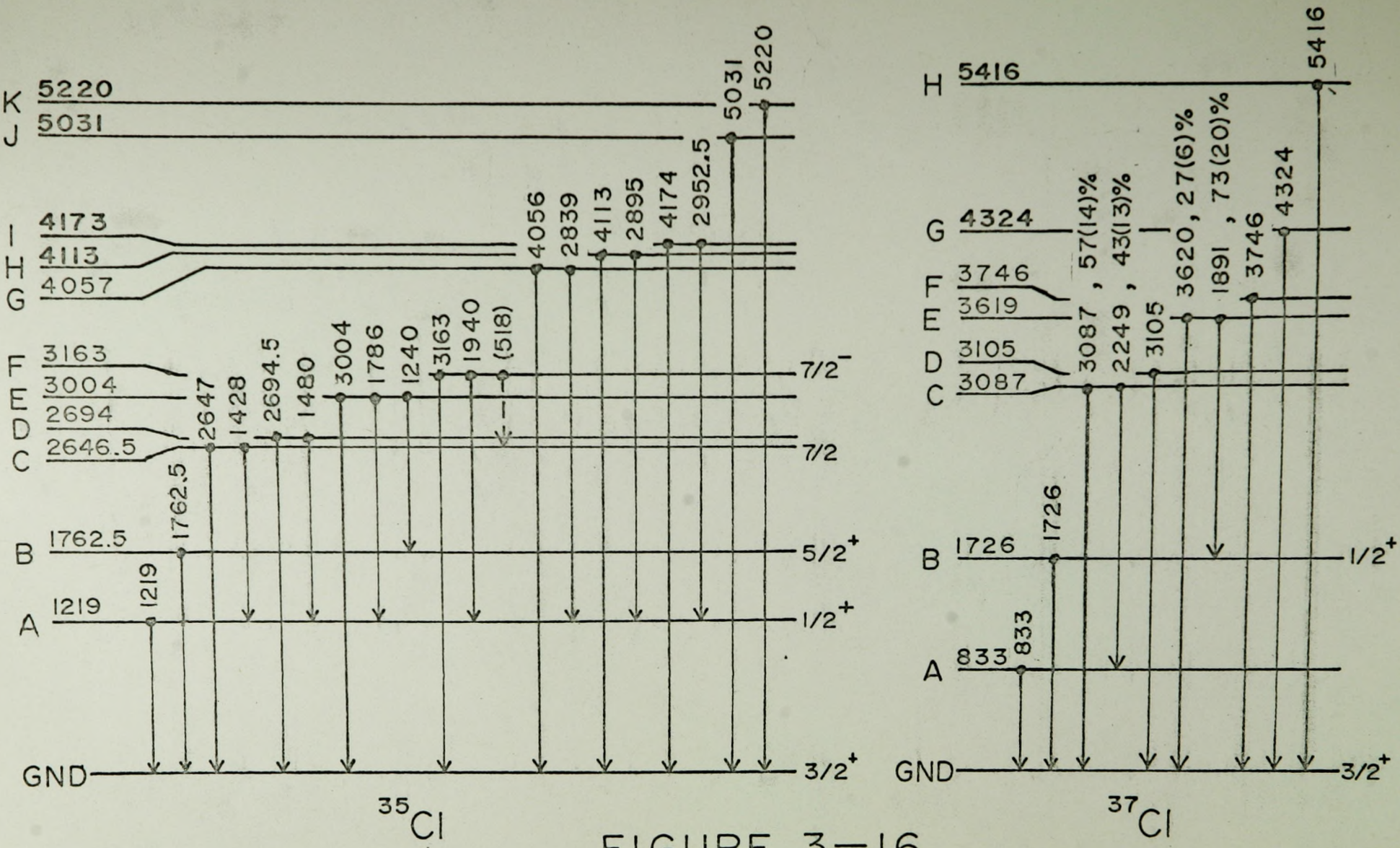

FIGURE 3—16

TABLE III-17

^{35}Cl BRANCHING RATIOS

Level	Present Work			Endt et al[8]		Endt et al[7]
	Level Energy*	Decay γ-rays	Branching Ratio+	Level Energy	Branching Ratio	Branching Ratio
A	1219 (4)			1220 (3)		
		1219 (4)	100	GND	100	
B	1762.5(4)			1762 (3)		
		1762.5 (4)	100	GND	100	
C	2646.5(4)			2645 (5)		
		2647 (5)	80 (7)	GND	75	40
		1427.5 (3)	20 (7)	A		60
				B	25	
D	2694.5 (4)			2695 (5)		
		2694.5 (4)	72 (5)	GND	35	80
		1480 (3)	28 (10)	A	65	20
E	3004 (4)			3006 (5)		
		3004 (8)	57 (5)	GND	100	
		1786 (3)	17 (10)	A	<10	
		1240 (3)	26 (7)	B	<10	
F	3163 (4)			3163 (5)		
		3163 (4)	71 (6)	GND	90	
		1940 (3)	29 (8)	A		
		(518)		C	10	
G	4057 (4)			4058 (5)		
		4056 (4)	22 (9)	GND	20	20
		2839 (4)	78 (22)	A	65	70
				D	15	10
H	4113 (4)			4113 (5)		
		4113 (4)	49 (12)			
		2895 (5)	51 (28)			
I	4173 (3)			4175 (5)		
		4174 (4)	53 (10)	GND	60	50
		2952.5 (3)	47 (18)	A	40	50
J	5031 (4)			5030 (50)		
		5031 (4)	100	GND	100	
K	5220 (6)			5220 (40)		
		5220 (6)	100	GND	100	

* All energies and errors, ( ), in keV

\+ Branching ratios and errors, ( ), in %

in Table III-17. There is quite good agreement on energy levels but some large disagreements on branching ratios. Level C tends to support the magnitudes of (8) but applied to the transitions reported in (7). Likewise (7) is supported by level D. The 518 keV γ-ray called for from level F is buried in the 511 keV annihilation peak and cannot, therefore, be checked by this experiment. Because of statistical and intensity considerations determination of the missing transition from level C is questionable.

The decay scheme for ^{37}Cl assigns the values 3619, 3746, 4324 and 5416 keV, respectively, to the reported levels (8) of 3.62, 3.74, 4.3 and 5.4 Mev. Likewise a level at 833 keV has been assigned as reported in (7) and (10) but not in (8). The branching ratios as seen for the levels shown are included in Figure 3-16. There were no report values for these in the references checked other than that the doublet at 3 Mev is reported to decay to the ground state in (7), (8) and (10).

Previous inelastic neutron scattering data reports only the first two levels of ^{35}Cl (10).

(c) Primary Population of Levels

The relative and corrected primary population values for ^{35}Cl and ^{37}Cl are tabulated in Table III-18 and III-19 respectively. The semi-logarithmic plots of relative primary yields in Figure 3-17 and 3-18 are inconclusive since insufficient spin data is available. However, the corrected value plots of Figures 3-19 (a + b), when compared with similar plots for ^{27}Al and ^{31}P can have spin assignments as shown. These then enable one to hazard the predictions given in Tables III-18 and III-19.

TABLE III-18

PRIMARY POPULATION VALUES FOR ^{35}Cl

Level	Energy (keV)	Spin (from (8))	Relative Primary Population Value	Corrected Values
GND		$3/2^+$		
A	1219	$1/2^+$	354 (139)	728 (284)
B	1762.5	$5/2^+$	847 (40)	2416 (114)
C	2646.5	7/2	266 (39)	1300 (190)
D	2694.5	[?]	195 (30)	975 (150)
E	3004	$[7/2^+]$	219 (49)	1330 (300)
F	3163	$7/2^-$	301 (43)	2005 (286)
G	4057	[1/2]	58 (18)	660 (205)
H	4113	[1/2]	43 (17)	506 (200)
I	4173	[1/2]	60 (17)	730 (207)
J	5031	[3/2]	15 (4)	306 (82)
K	5220	[3/2]	10 (4)	227 (91)

[ ] Spins predicted from Fig. 3-19.

TABLE III-19

^{37}Cl PRIMARY POPULATION VALUES

Level	Energy (keV)	Spin from (8)	Relative Primary Population Value	Corrected Values
GND	0	$3/2^+$		
A	833		71 (11)	117 (18)
B	1726	$1/2^+$	188 (24)	522 (67)
C	3087	7/2	217 (60)	1357 (375)
D	3105	5/2	120 (30)	775 (194)
E	3619	5/2	112 (29)	974 (250)
F	3746	3/2	38 (7)	358 (66)
G	4324	5/2 7/2	110 (49)	1448 (645)
H	5416	1/2	25 (4)	640 (103)

spins predicted from Fig. 3-19.

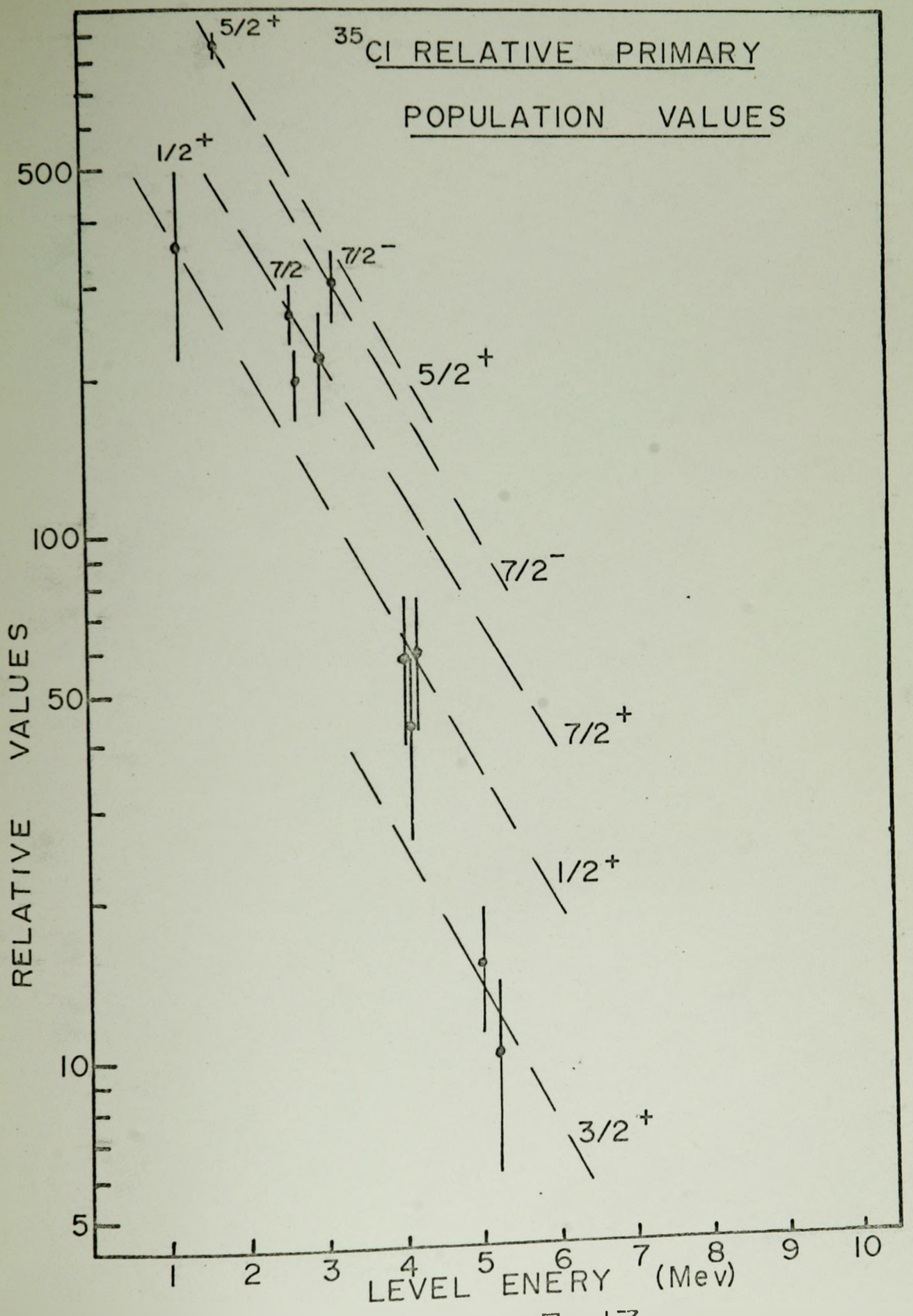
^{35}Cl RELATIVE PRIMARY
POPULATION VALUES
5/2+
1/2+
7/2
7/2−
5/2+
7/2−
7/2+
1/2+
3/2+
RELATIVE VALUES
500
100
50
10
5
1
2
3
4
5
6
7
8
9
10
LEVEL ENERY (Mev)

FIGURE 3-17

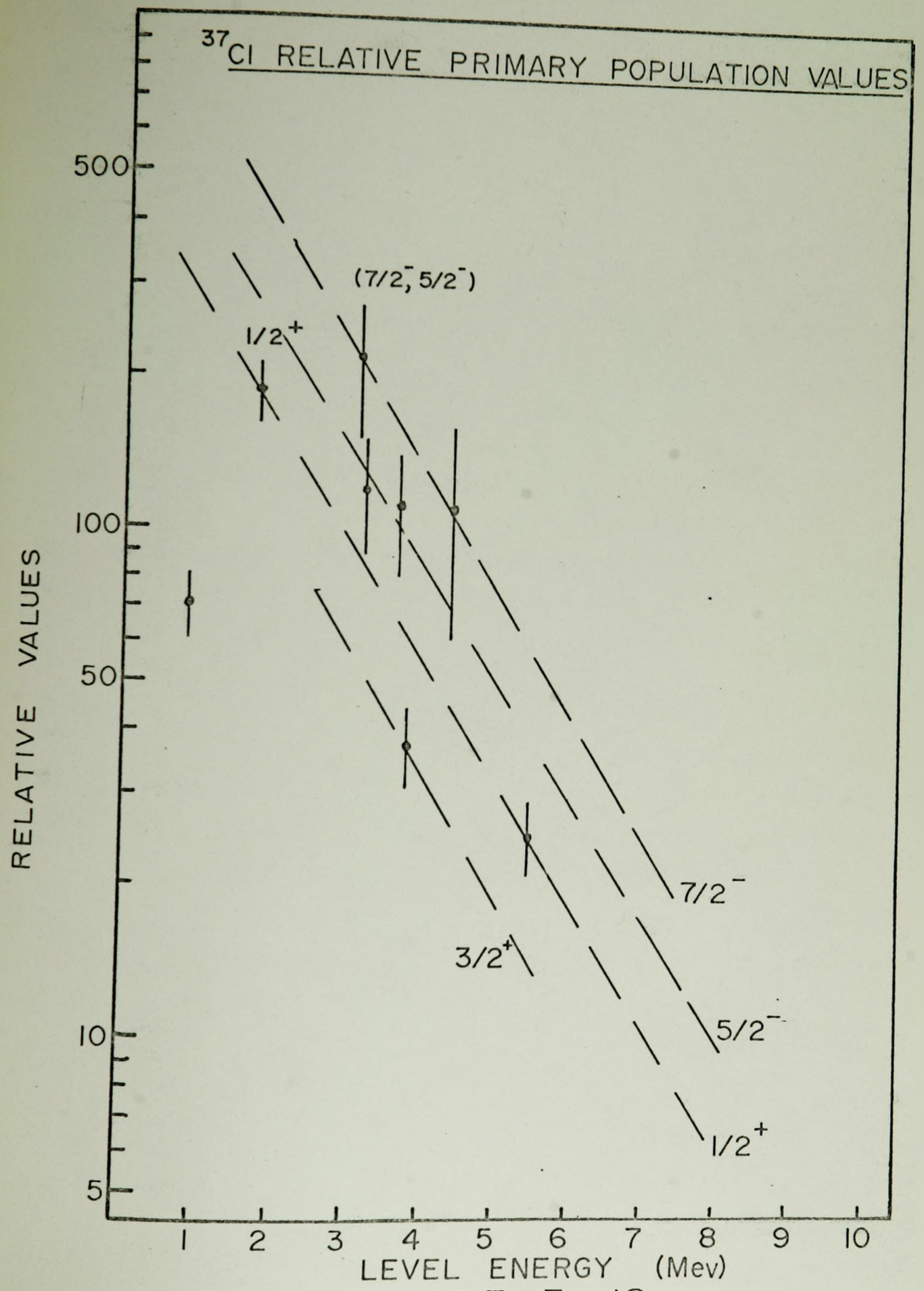
^{37}Cl RELATIVE PRIMARY POPULATION VALUES
500
100
50
10
5
RELATIVE VALUES
(7/2⁻, 5/2⁻)
1/2⁺
7/2⁻
3/2⁺
5/2⁻
1/2⁺
1
2
3
4
5
6
7
8
9
10
LEVEL ENERGY (Mev)

FIGURE 3—18

^{35}Cl AND ^{37}Cl CORRECTED RELATIVE POPULATION VALUES

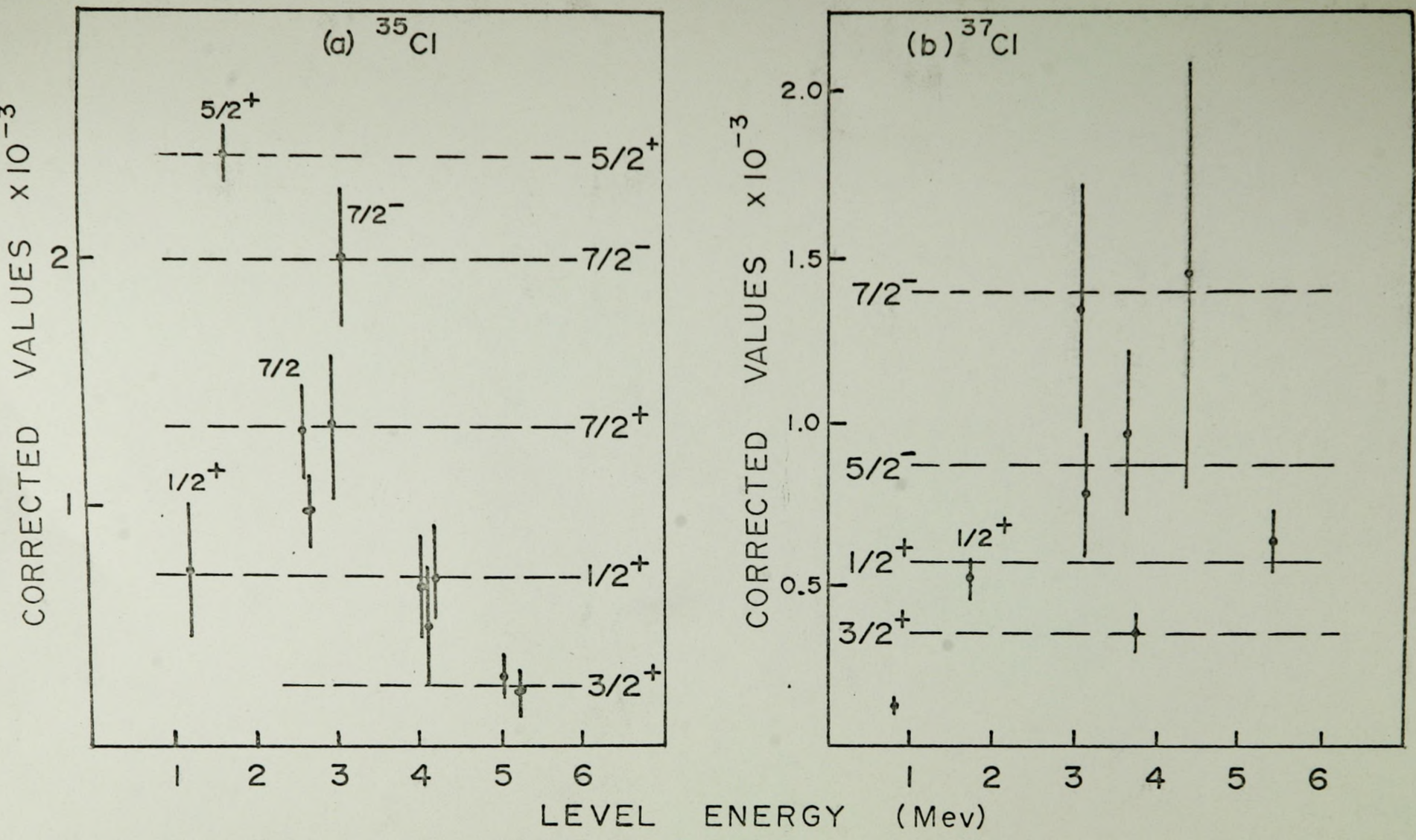

FIGURE 3—19

IV CONCLUSIONS

The results of these experiments indicate that using reactor neutrons for inelastic scattering studies of nuclei is a very viable method now that high resolution γ-ray detectors are available. Even with the "damaged" detector used the resolution and intensities allowed one to confirm or deny most of the previously reported work done by the (p, p', γ) method. In fact, with a beam port designed especially for neutron inelastic scattering and a higher resolution detector one should be able to do coincidence experiments to confirm many of the questionable assignments in the previous work.

The methods used in this work to investigate the spin and parity assignments of the various excited states seem to indicate that one could use Donahue's method for first approximations if one had the better statistics that a facility specifically designed for this work would allow. Likewise Feshbach's method may give better agreement if one had not made the simplification to his formula (see Section 1.3).

REFERENCES

(1) Hauser, W. and Feshbach, H., Phys. Rev. 87, No. 2, 366 (1952)

(2) Donahue, D. J., Phys. Rev. 128, No. 3, 1231 (1962)

(3) Johns, M. W. and Hughes, L. B., Research Reactor Journal 2 No. 4, 11 (1962)

(4) Fiedler, H. J., Hughes, L. B., Kennett, T. J., Prestwich, W. V., and Wall, B. J., Nucl. Inst. and Methods 40, No. 2, 229 (1966)

(5) U.S.A.E.C., Research Reactors, McGraw-Hill, N. Y. 1955, pp 107-112.

(6) Lycklama, H., Hughes, L. B., and Kennett, T. J., Can. Journ. of Phys., 45, 1871 (1967)

(7) Endt, P. M., and VanderLeun, C., Nuc. Phys. 34, No. 1 (1962)

(8) Endt, P. M., and VanderLeun, C., Nuc. Phys. A105, No. 1 (1967)

(9) Nichol, L. N., and Kennett, T. J., to be published (1968)

(10) Nuclear Data Sheets, compiled by K. Way et al. (N.A.S. - N.R.C., Washington 25, D. C.)

(11) Mathur, S. C., Tucker, W. E., Benjamin, R. W., and Morgan, I. L., Nuc. Phys. 73, No. 3, 561 (1965)

(12) Blizard, E. P., and Abbot, L. S., Reactor Handbook Vol. IIIB, Interscience, N. Y. 1962, pp 18 and 19

(13) Norman, G. R., private communication.